Coseismic slip distribution of the 2011 off the Pacific Coast of Tohoku Earthquake (M9.0) refined by means of seafloor geodetic data

T. Iinuma,[1,2] R. Hino,[1] M. Kido,[1,2] D. Inazu,[1,3] Y. Osada,[1,2] Y. Ito,[1] M. Ohzono,[4] H. Tsushima,[5] S. Suzuki,[1] H. Fujimoto,[1,2] and S. Miura[6]

Received 27 January 2012; revised 28 May 2012; accepted 8 June 2012; published 26 July 2012.

[1] On 11 March 2011, the devastating M9.0 Tohoku Earthquake occurred on the interface of the subducting Pacific plate, and was followed by a huge tsunami that killed about 20,000 people. Several geophysical studies have already suggested that the very shallow portion of the plate interface might have played an important role in producing such a large earthquake and tsunami. However, the sparsity of seafloor observations leads to insufficient spatial resolution of the fault slip on such a shallow plate interface. For this reason, the location and degree of the slip has not yet been estimated accurately enough to assess future seismic risks. Thus, we estimated the coseismic slip distribution based on terrestrial GPS observations and all available seafloor geodetic data that significantly improve the spatial resolution at the shallow portion of the plate interface. The results reveal that an extremely large (greater than 50 m) slip occurred in a small (about 40 km in width and 120 km in length) area near the Japan Trench and generated the huge tsunami. The estimated slip distribution and a comparison of it with the coupling coefficient distribution deduced from the analysis of the small repeating earthquakes suggest that the 2011 Tohoku Earthquake released strain energy that had accumulated over the past 1000 years, probably since the Jogan Earthquake in 869. The accurate assessments of seismic risks on very shallow plate interfaces in subduction zones throughout the world can be obtained by improving the quality and quantity of seafloor geodetic observations.

Citation: Iinuma, T., et al. (2012), Coseismic slip distribution of the 2011 off the Pacific Coast of Tohoku Earthquake (M9.0) refined by means of seafloor geodetic data, *J. Geophys. Res.*, *117*, B07409, doi:10.1029/2012JB009186.

1. Introduction

[2] Many large earthquakes of magnitude 7 ∼ 8 have been recurring on the plate interface beneath the northeastern Japanese Islands (Figure 1). These earthquakes release the strain energy that accumulates due to interplate coupling between the continental (North American or Okhotsk) plate and the Pacific plate, which is subducting in the Japan Trench at a rate as 7.0 ∼ 8.5 mm/year [*Altamimi et al.*, 2007]. Based on previous geophysical and geological investigations, the Japanese government's Headquarters for Earthquake Research Promotion has documented the specific probability of earthquakes that occur on each segment of the plate boundary in this subduction zone (2011, http://jishin.go.jp/main/choukihyoka/ichiran_past/ichiran20110111.pdf, in Japanese). Even though earthquakes that result from the rupture of not only single but also multiple segments are considered, no evaluation is performed for earthquakes of magnitude larger than 8.5 at the NE Japan subduction zone.

[3] However, an M 9.0 earthquake, the 2011 off the Pacific Coast of Tohoku Earthquake (or 2011 Tohoku Earthquake), has occurred on 11 March 2011, and a huge tsunami associated with the earthquake wiped out about 20,000 people. Many studies have investigated the source process and slip distribution of this huge earthquake based on seismological and geodetic data, and revealed that the M9 earthquake has ruptured not only deep (40 ∼ 50 km in depth) portion of the plate interface but also the shallow (≤30 km in depth) plate interface with large (≥20 m) slip amount [e.g., *Ide et al.*, 2011; *Ito et al.*, 2011a; *Koketsu et al.*, 2011; *Koper et al.*, 2011; *Pollitz et al.*, 2011; *Simons et al.*, 2011]. However, the differences of the coseismic slip distributions in very shallow part (≤15 km in depth) among the previous models are significantly large. The ranges of the slipped areas and maximum

[1]Research Center for Predictions of Earthquakes and Volcanic Eruptions, Graduate School of Science, Tohoku University, Sendai, Japan.
[2]Now at International Research Institute of Disaster Sciences, Tohoku University, Sendai, Japan.
[3]Now at National Research Institute for Earth Science and Disaster Prevention, Tsukuba, Japan.
[4]Institute of Seismology and Volcanology, Graduate School of Science, Hokkaido University, Sapporo, Japan.
[5]Meteorological Research Institute, Japan Meteorological Agency, Tsukuba, Japan.
[6]Earthquake Research Institute, University of Tokyo, Tokyo, Japan.

Corresponding author: T. Iinuma, Research Center for Predictions of Earthquakes and Volcanic Eruptions, Graduate School of Science, Tohoku University, 6-6 Aza-Aoba, Aramaki, Aoba-Ku, Sendai, Miyagi 980-8578, Japan. (iinuma@irides.tophoku.ac.jp)

0148-0227/12/2012JB009186

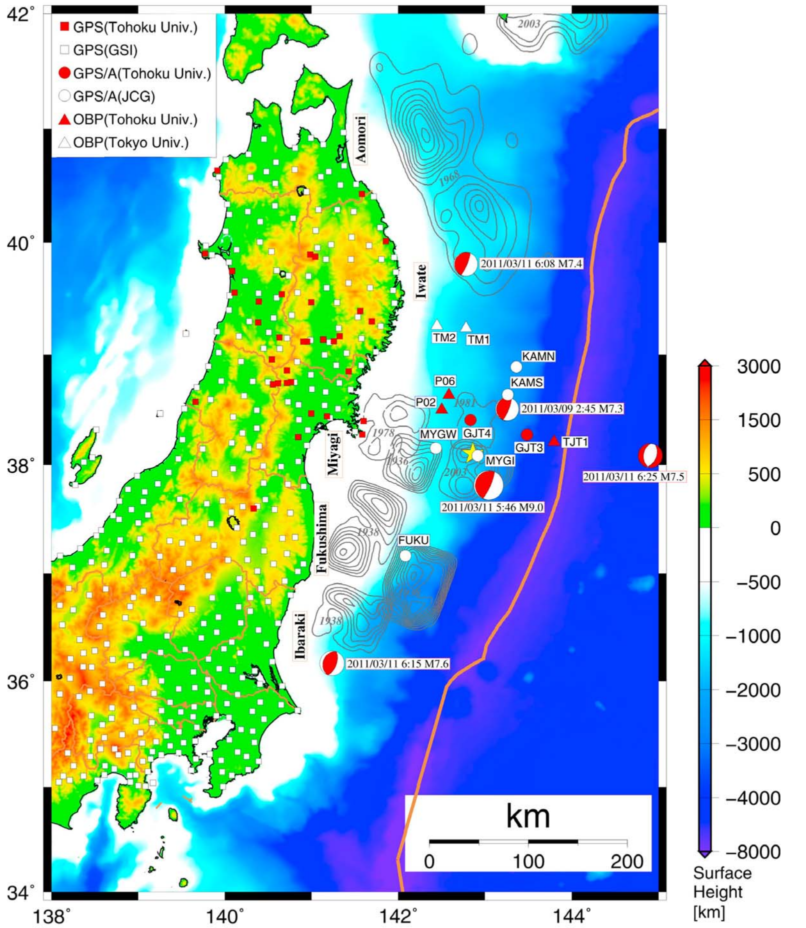

Figure 1. Map of the study area. Squares, circles and triangles indicate the terrestrial GPS, seafloor GPS/A and OBP sites, respectively. Red symbols correspond the sites of Tohoku University, while white symbols represent the sites of other organizations (terrestrial GPS sites of GSI, seafloor GPS/A sites of JCG, and OBP stations of the University of Tokyo). Codes of the seafloor stations are written. The locations of the centroids of the main shock, the largest foreshock (9 March 2011, M7.3), and three large aftershocks that occurred on 11 March 2011 (M7.4 off Iwate Prefecture, M7.5 far off Miyagi Prefecture and M7.6 off Ibaraki Prefecture) are indicated along with their focal mechanisms determined by JMA [*Hirose et al.*, 2011]. The hypocenter of the main shock is pointed by a yellow star. The gray contours denote the slip areas for recent major earthquakes at Tokachi-oki in 2003 (M8.0) and 1968 (M7.9), Miyagi-oki in 1978 (M7.4), 1981 (M7.0) and 1936 (M7.4), and Fukushima-oki in 2003 (M7.1) and 1938 (M7.3, M7.4 and M7.5) [*Murotani*, 2003; *Yamanaka and Kikuchi*, 2003, 2004] (http://www.eri.u-tokyo.ac.jp/sanchu/Seismo_Note/EIC_News/031031.html). The brown lines denote the prefectural borders and the trench axis. The names of prefectures along the Pacific coast (Aomori, Iwate, Miyagi, Fukushima, and Ibaraki) are presented along their coasts.

slip amounts are not corresponding with each other because spatial resolution of the inversion analyses are not enough to constrain the slip on the plate interface near the trench as long as we perform the analyses based on seismological and geodetic data that are observed at terrestrial sites. Several displacements at seafloor geodetic observation sites are included by *Ito et al.* [2011a], *Koketsu et al.* [2011] and *Pollitz et al.* [2011], but the densities of the observation points are also insufficient to resolve the slip along the trench.

[4] In spite of such poor resolvability, we need to estimate the slip distribution associated with the 2011 Tohoku Earthquake with high accuracy to understand the preparation and generation processes of the huge earthquake and tsunami. Where and how large did the coseismic slip occur on the plate interface, especially at the very shallow portion? Does the slip amount balance with the slip deficit that is accumulated during the interseismic period due to the plate convergence and interplate coupling? To tackle these problems, we involved the new seafloor observation data into the geodetic inversion analysis to estimate the slip distribution of the 2011 Tohoku earthquake.

2. Data and Analysis

2.1. Observations and Coseismic Displacements Estimation

[5] We analyzed the coseismic displacements due to the 2011 off the Pacific Coast of Tohoku Earthquake to

Table 1. Date of Observations and Estimated Coseismic Displacements at GPS/A Stations After *Kido et al.* [2011] (GJT3 and GJT4) and *Sato et al.* [2011]

Station Code	Date of Observation (UTC)		Coseismic Displacement[a] (m)		
	Pre-Tohoku Earthquake	Post-Tohoku Earthquake	Easting	Northing	Vertical
GJT3	1 November 2005	11 April 2011	29.5 ± 0.5	−11 ± 0.5	3.9 ± 0.5
GJT4	11 April 2010	11 April 2011	14 ± 1	−5 ± 1	N/A
MYGI	21 February 2011	28 March 2011	22.1 ± α	−10.4 ± α	3.1 ± α
MYGW	21 February 2011	28 March 2011	14.3 ± α	−5.1 ± α	−0.8 ± α
FUKU	23 February 2011	29 March 2011	4.4 ± α	−1.7 ± α	0.9 ± α
KAMN	16 November 2010	3 April 2011	13.8 ± β	−5.8 ± β	1.6 ± β
KAMS	19 November 2010	5 April 2011	21.1 ± β	−8.9 ± β	1.5 ± β

[a] $\alpha = 0.1 \sim 0.2$ and $\beta = 0.5 \sim 0.6$.

estimate the coseismic slip distribution of the earthquake. The displacements at geodetic observation stations are estimated based on the terrestrial Global Positioning System (GPS) observations, seafloor GPS/Acoustic (GPS/A) ranging, and the change in the seafloor water pressure recorded by means of Ocean Bottom Pressure gauges (OBPs). GPS and OBP data are continuous while GPS/A observations are carried out by campaigns with research vessels.

2.1.1. Terrestrial GPS Observation

[6] Tohoku University have been carrying out continuous terrestrial Global Positioning System (GPS) observations to investigate the earthquake generation processes of interplate earthquakes that have repeatedly occurred at the plate boundary offshore the Tohoku district since 1987 [*Miura et al.*, 1993]. The GPS observation network of Tohoku University spatially interpolates the nationwide GPS network, GEONET, which has been being managed by Geospatial Information Authority of Japan (GSI) [*Miyazaki and Hatanaka*, 1998].

[7] We can improve the spatial resolution of the inversion analysis to estimate the coseismic slip distribution especially around the Miyagi-oki region by using GPS data observed at 383 sites of not only GSI (345 sites) but also Tohoku University (38 sites). *Ohzono et al.* [2012] estimated daily coordinates before and after the main shock by using Bernese GPS Software version 5.0 [*Dach et al.*, 2007], and calculated coseismic displacements by taking the differences between daily site coordinates before and after the main shock, namely on March 10 and 11 (after 5:47 on GPS time). Refer to *Ohzono et al.* [2012] for the further detail of GPS observation and data processing. This displacement field deduced from terrestrial GPS observation is used in this study as well as *Iinuma et al.* [2011].

2.1.2. Seafloor GPS/A Ranging

[8] We have been performing seafloor crustal deformation observations using GPS/A off the Tohoku district. We can estimate the coseismic horizontal displacement at the seafloor stations by comparing the positions of the stations before and after earthquake. *Kido et al.* [2011] reported the displacements of 20 ∼ 30 m at GPS/A stations of Tohoku University, named GJT3 and GJT4. Japan Coast Guard (JCG) has also performed GPS/A observations at 5 stations in this region and has already reported the coseismic displacements at their sites [*Sato et al.*, 2011]. A total of 7 GPS/A stations had been available when the 2011 Tohoku earthquake occurred, and we can use displacements at all the GPS/A stations to estimate the coseismic slip distribution on the plate interface. Details concerning the GPS/Acoustic observations and data processing methods are given by *Kido et al.* [2011] and *Sato et al.* [2011]. Table 1 summarizes observation dates and estimated seafloor displacements at the GPS/A stations. Note that the displacements at GPS/A stations include the displacements due to the postseismic processes associated with the 2011 Tohoku earthquake because the GPS/A observation is not continuous but campaign style.

2.1.3. OBP Measurement

[9] The second type of the seafloor observation is OBP. Vertical displacement due to the earthquake causes the abrupt change in OBP at each OBP station that has been installed at seafloor. Before the 2011 Tohoku Earthquake occurred, 12 OBP gauges had been installed on the seafloor off the Tohoku district by Tohoku University and the Earthquake Research Institute (ERI) of the University of Tokyo. Since the gauges installed by Tohoku University are off-line type gauges, named P02, P06, GJT3, and TJT1, it is necessary to issue acoustic commands from a surface vessel in order to retrieve the OBP gauge from the seafloor. The method of estimating the coseismic displacement from the continuous OBP records is described by *Hino et al.* [2011] and *Ito et al.* [2011b].

[10] As they presented, the pressure-gauge data include the effects of the ocean tide, flows of the seawater, instrumental drift, strong ground motions induced by the seismic waves, and tsunamis other than large offsets due to the coseismic slip. The ocean tides were precisely estimated by means of a harmonic analysis applying BAYTAP-G [*Tamura et al.*, 1991] and were removed from the original records. The movement of the oceanic layer was estimated by a global barotropic ocean model forced by synoptic atmospheric disturbances and its contribution to the seafloor pressure was subtracted from the tide-free pressure data. Drift components can be approximated by linear functions with steady drift rates that are calculated from the pressure records before March 8, 2011. After removing these components, we converted the pressure data to seafloor level using constant seawater density as 1,030 kg/m^3. Figure 2 shows the time series of the change in seafloor level at each site. We can estimate coseismic seafloor vertical displacements based on the step amounts of the time series without including any postseismic deformation. Table 2 shows the estimated coseismic displacements.

[11] The OBP records obtained using the ERI cabled OBP gauges off Iwate Prefecture, named TM1 and TM2, have been reported by *Maeda et al.* [2011]. These records (shown in Figure 8) are broken about 30 min after the main shock

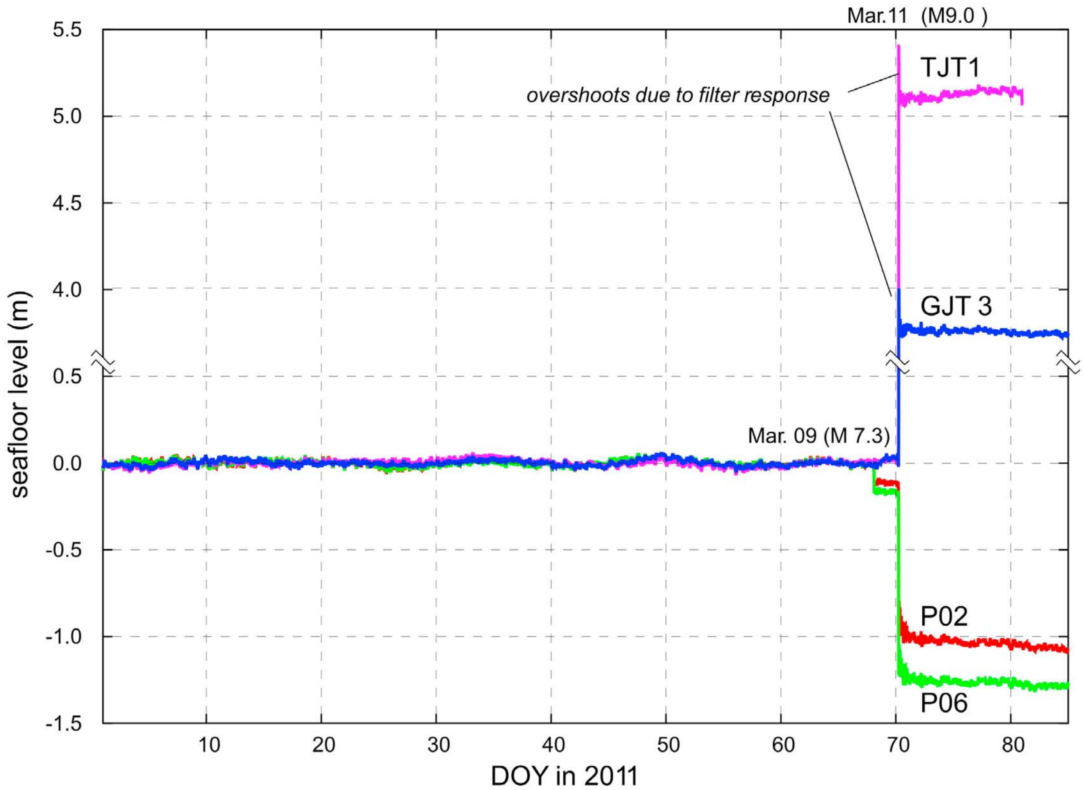

Figure 2. Time series of the seafloor levels from Jan. 1 to Mar. 26, 2011. A zero-phase low-pass filter with a cutoff period of 2 hours was applied to all the traces to reduce the short period and large amplitude oscillations caused by earthquakes and tsunamis. The overshoots immediately after the main shock appearing in the traces for GJT3 and TJT1 were due to the filter response.

occurrence, but subsidence of the seafloor level (increase in the sea surface level) is apparent at both sites. Estimated subsidence are 0.8 ± 0.2 m and 0.3 ± 0.2 m for TM1 and TM2, respectively.

2.2. Inversion Analysis

[12] We applied the inversion method summarized by *Iinuma* [2009] to estimate the coseismic slip distribution on the plate boundary fault based on the displacement field. In this inversion method, the weights of three constraint conditions, namely, spatial smoothing, initial damping value, and the boundary condition are optimized by minimizing Akaike's Bayesian Information Criterion (ABIC) [*Akaike*, 1977, 1980]. Refer to appendix for the detail of the inversion method. We applied a plate boundary model developed by *Nakajima and Hasegawa* [2006] to model the plate interface fault. The spatial distribution of the fault slip is represented by the superposition of normalized bi-cubic B-splines, distributed at 20-km intervals. The number of the node points of the spline functions is also optimized based on ABIC.

[13] To calculate the green's function between the fault slip and surface displacement, we assumed homogenous elastic half-space with $\lambda/\mu = 1.0$, where λ and μ are Lamé parameters. The depths of seafloor are taken into account by changing the depth of the plate interface fault when we calculate the green's functions for seafloor stations. For instance, we used $(z(x, y) - z_0)$ km for the depth of the plate interface fault to calculate the green's function of the seafloor station that is installed at a depth of z_0 km underwater, where the depth of the plate interface defined as a function of the longitude, x, and latitude, y, namely, $z(x, y)$.

[14] Vertical and horizontal displacements at terrestrial GPS sites are equally weighted in the inversion analysis, because modeling errors due to the uncertainty and heterogeneity of physical properties of the crust such as rigidity and Poisson's ratio, errors in the geometry of the plate interface fault, and the effect of terrain topography, almost certainly exceed the observation errors at most of the GPS stations. In particular, observation errors of GPS measurements on land are less than 5 and 20 mm for horizontal and vertical components, respectively [e.g., *Ozawa et al.*, 2011], while 10% of modeling error (cf. spatial variations of Vs and

Table 2. Vertical Displacements Estimated From the OBP Records

Station Code	Displacement (m)	Estimation Error (m)
P02	−0.801	0.016
P06	−0.975	0.015
GJT3	3.734	0.012
TJT1	5.093	0.014
TM1	−0.8	0.2
TM2	−0.3	0.2

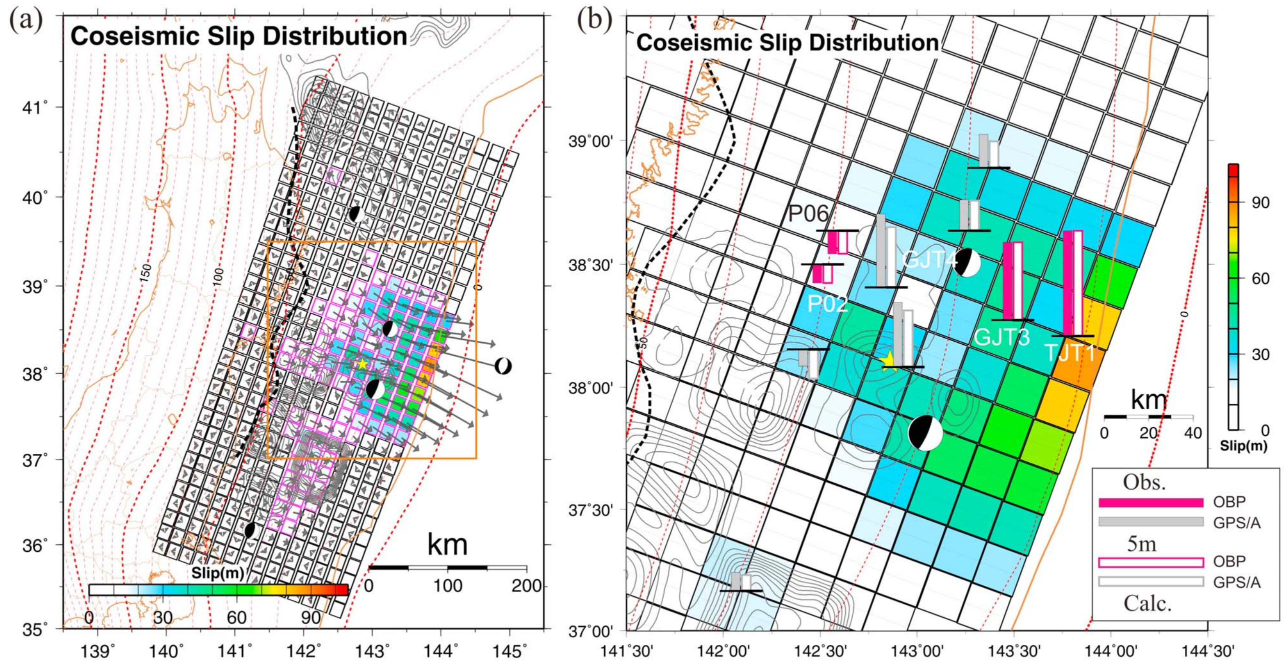

Figure 3. Estimated coseismic slip distribution. (a) Arrows denote slip vectors on the hanging wall of the plate interface. The squares outlined in purple indicate regions where the estimated slip values are greater than the estimation errors (Figure 4a). The black dashed line denotes the down-dip limit of interplate earthquakes determined by *Igarashi et al.* [2001]. The broken red lines show the depth of the subducting plate interface [*Nakajima and Hasegawa*, 2006]. An orange rectangle corresponds the range of the Figure 3b. (b) Enlarged view of the coseismic slip distribution off Miyagi Prefecture and the comparison between observed vertical displacements (solid bars) and calculated ones (white bars) from the estimated coseismic slip distribution at seafloor stations. Red and gray bars correspond the displacements at the OBP and GPS/A stations, respectively. Codes of Tohoku University's seafloor stations are written.

Vp/Vs [e.g., *Nakajima et al.*, 2001; *Yamamoto et al.*, 2011]) exceeds 100 mm for the calculated displacement that is larger than 1 m (Most of GPS sites in Tohoku district moved more than 1 m). Although there are two vertical displacement measurements at GJT3 by means of both GPS/A and OBP, vertical displacement at GJT3 measured by GPS/A is not used for the inversion analysis because the accuracy of the measurement is worse than the OBP measurement, and because the difference between these displacement data is not significant taking observation errors into account. Optimization of the weights of the displacement data based on different observation procedures is important. We attempted to perform this optimization based only on ABIC, but this did not work well because the seafloor site distribution is too sparse. Therefore, we subjectively weighted the OBP data more strongly than other data (10^4 times heavier compared to GPS displacement), because the vertical displacements estimated from the OBP time series data include only the coseismic deformation, while the displacements at the GPS and GPS/A stations include postseismic deformations and displacements due to the aftershocks that occurred on 11 March 2011.

3. Results and Discussion

3.1. Estimated Coseismic Slip Distribution

[15] The estimated slip vectors on the hanging wall of the plate interface are shown in Figure 3a. The squares outlined in purple represent locations where significant slip has occurred, with slip values larger than the estimation error (Figure 4).These can be generally divided into three different areas. The first is the primary rupture area (PRA) surrounding the hypocenter and extending to the east; this is characterized by slip values of greater than 20 m and includes an area of very large (≥50 m) slip (VLSA) near the Japan Trench (Figure 3b). The maximum slip is about 85 m, and the VLSA is about 120 km long and 40 km wide. The PRA itself extends about 160 km in the direction parallel to the trench axis, and about 120 km in the direction normal to the trench. The PRA is located at the plate interface at a depth of less than 30 km, where the subducting plate mainly contacts the crust of the continental plate [*Ito et al.*, 2005; *Yamamoto et al.*, 2011]. Our result further suggests that the area where the coseismic slip reached the earth surface is not as broad as previous studies suggested [*Ide et al.*, 2011; *Simons et al.*, 2011; *Maeda et al.*, 2011].

[16] The second area where significant slip is estimated is a region off Fukushima Prefecture which overlaps the rupture areas of earthquakes that occurred in 1938 [*Murotani*, 2003]. Several studies estimated large slip at almost same areas off Fukushima Prefecture based on seismic waveform analyses [*Ammon et al.*, 2011; *Koketsu et al.*, 2011; *Yagi and Fukahata*, 2011]. This area extends to the south, off Ibaraki Prefecture, and reflects displacements measured at terrestrial GPS and seafloor GPS/A sites, including the crustal deformation due to the M7.7 aftershock off Ibaraki Prefecture,

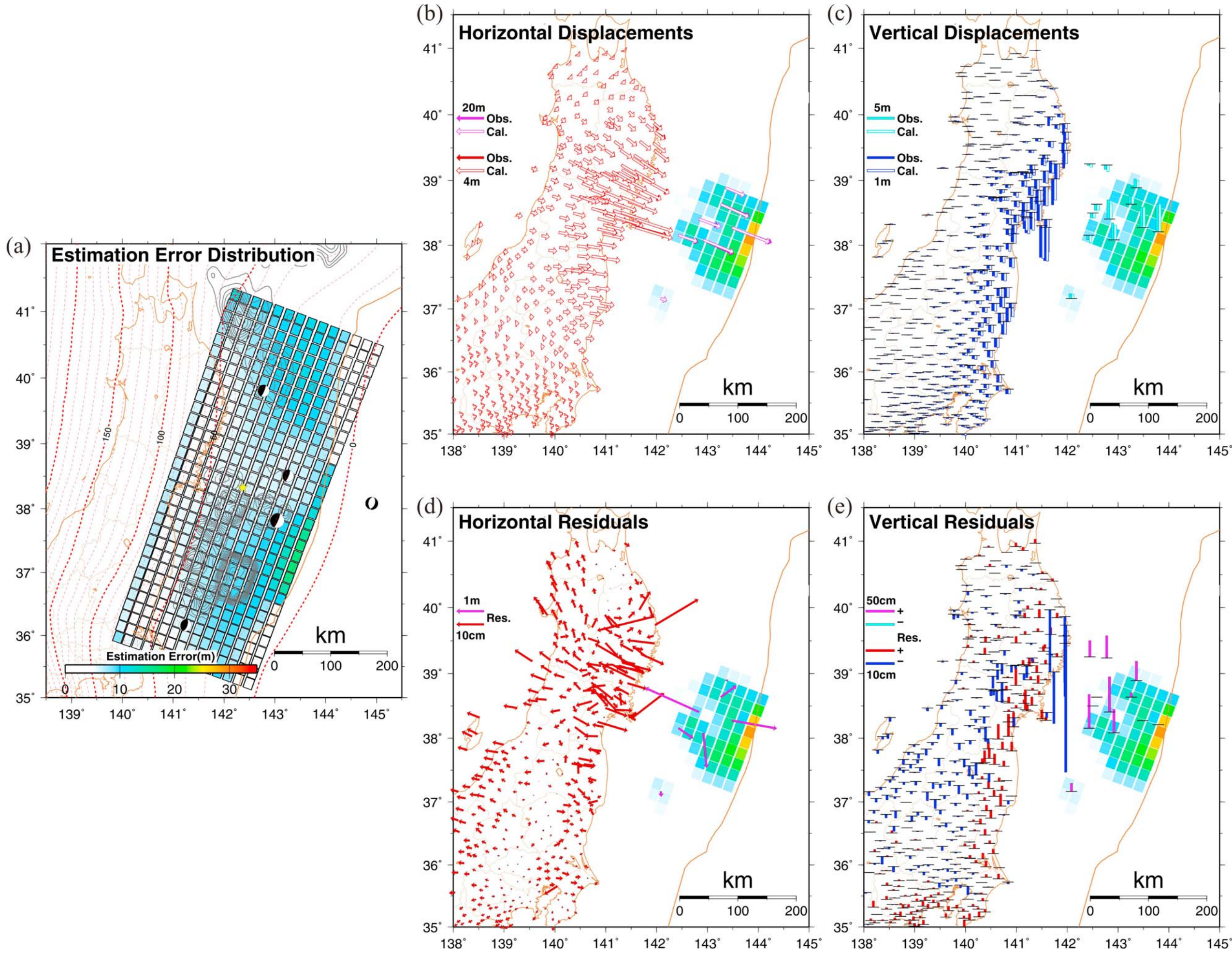

Figure 4. Result of the inversion analysis. (a) The distribution of the error of estimated coseismic slip. (b) Comparison between observed horizontal displacements (solid arrows) and calculated ones (white arrows) from the estimated coseismic slip distribution. Note that the scales for the terrestrial and seafloor sites are different. (c) Comparison between observed vertical displacements (solid bars) and calculated ones (white bars) from the estimated coseismic slip distribution. Note that the scales for the terrestrial and seafloor sites are different. (d) Horizontal components of the residuals. (e) Vertical components of the residuals. The residuals are determined by subtracting the calculated displacement from the observed displacement for each site.

which occurred about 30 min after the main shock. No significant slip is estimated for the very shallow (≤15 km in depth) or deep (≥40 km in depth) portions of the plate interface off and beneath Fukushima Prefecture, respectively.

[17] The third area of significant slip is located near the coast in the Miyagi-oki region where M $\sim$ 7.5 earthquakes have repeatedly occurred [*Seno et al.*, 1980; *Umino et al.*, 2006]. The estimated slip distribution suggests that the areas that ruptured during the earthquakes off Miyagi Prefecture in 1978 again ruptured during the 2011 Tohoku Earthquake, as suggested by *Iinuma et al.* [2011].

[18] The released moment based on the estimated slip distribution is 4.03×10^{22} Nm, which is equivalent to a moment magnitude (Mw) of 9.00 and almost identical to the value determined by the Japan Meteorological Agency. The released moment in the PRA and VLSA are respectively about 60% and 17% of the whole, namely, 2.44×10^{22} Nm and 6.84×10^{21} Nm (equivalent to Mw 8.86 and 8.49). The degree of slip is extremely large and the fault size is very small, based on the released seismic moment, when compared to the scaling laws deduced from previous earthquakes at the subduction zone around the Japanese Islands [*Fujii and Matsu'ura*, 2000; *Murotani et al.*, 2008]. *Murotani et al.* [2008] deduced scaling laws between rupture areas, seismic moments, average slips and combined areas of asperities for large (Mw 6.7 $\sim$ 8.4) earthquakes on the plate boundaries as shown in Figure 5 with those quantities of 2011 Tohoku earthquake estimated in this study. Subfaults with slip >1.5 times larger than the average slip over the rupture area with significant slip are regarded as an asperity in the figure. The comparisons with the previous earthquakes shown in Figure 5 clearly exhibit that not only the maximum but average of the coseismic slip is very large (Figure 5b) and that both rupture area and the combined

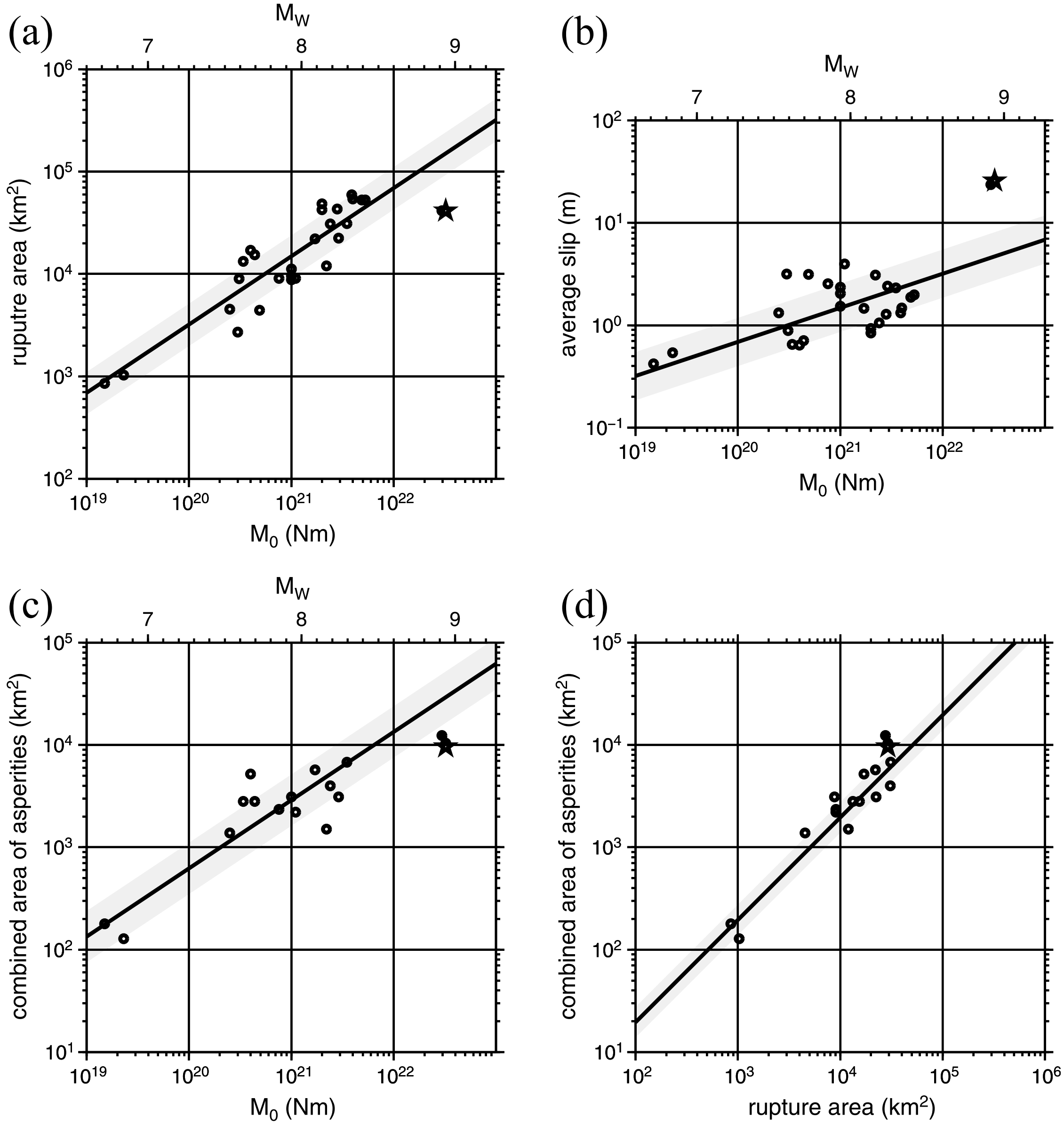

Figure 5. Scaling relationships of (a) rupture area, (b) average slip, and (c) combined area of asperities with respect to the seismic moment. (d) Relationship between combined area of asperities and rupture area after *Murotani et al.* [2008]. Shadow zones indicate standard deviations of 1.61 (Figure 7a), 1.72 (Figure 7b), 1.78 (Figure 7c), and 1.41 (Figure 7d). White circles denote data compiled by *Murotani et al.* [2008]. The quantities with respect to the 2011 off the Pacific coast of Tohoku earthquake are plotted by a white star (for the estimated coseismic slip distribution) and black circles (for the modified coseismic slip distributions) based on this study.

area of asperities are significantly small (Figures 5a and 7c). The ratio of the combined area of asperities to the whole rupture area is not so large (Figure 5d) implying that some kind of physical process, such as dynamic overshooting [*Ide et al.*, 2011] and/or strong velocity weakening at high slip velocities [*Shibazaki et al.*, 2011; *Mitsui and Iio*, 2011], strengthened the degree of slip not only on the asperities but also whole rupture area.

3.2. Examination of the Results

[19] We carried out several tests to assess the spatial resolution of our inversion analysis. First, we performed two types of computational tests to examine the spatial resolution of the inversion analysis, namely, the Checkerboard Resolution Tests (CRTs) and the Reconstruction Tests (RTs). Second, Additional inversion analyses were performed to check the dependence of the results on the distribution of the observation stations.

3.2.1. Resolution Tests

[20] The CRTs determine the spatial resolution for slip areas of certain wavelengths on the plate interface. In these tests, displacements at geodetic sites are calculated using slip distributions with a checkerboard pattern on the plate interface, and then the interplate slip distributions are estimated

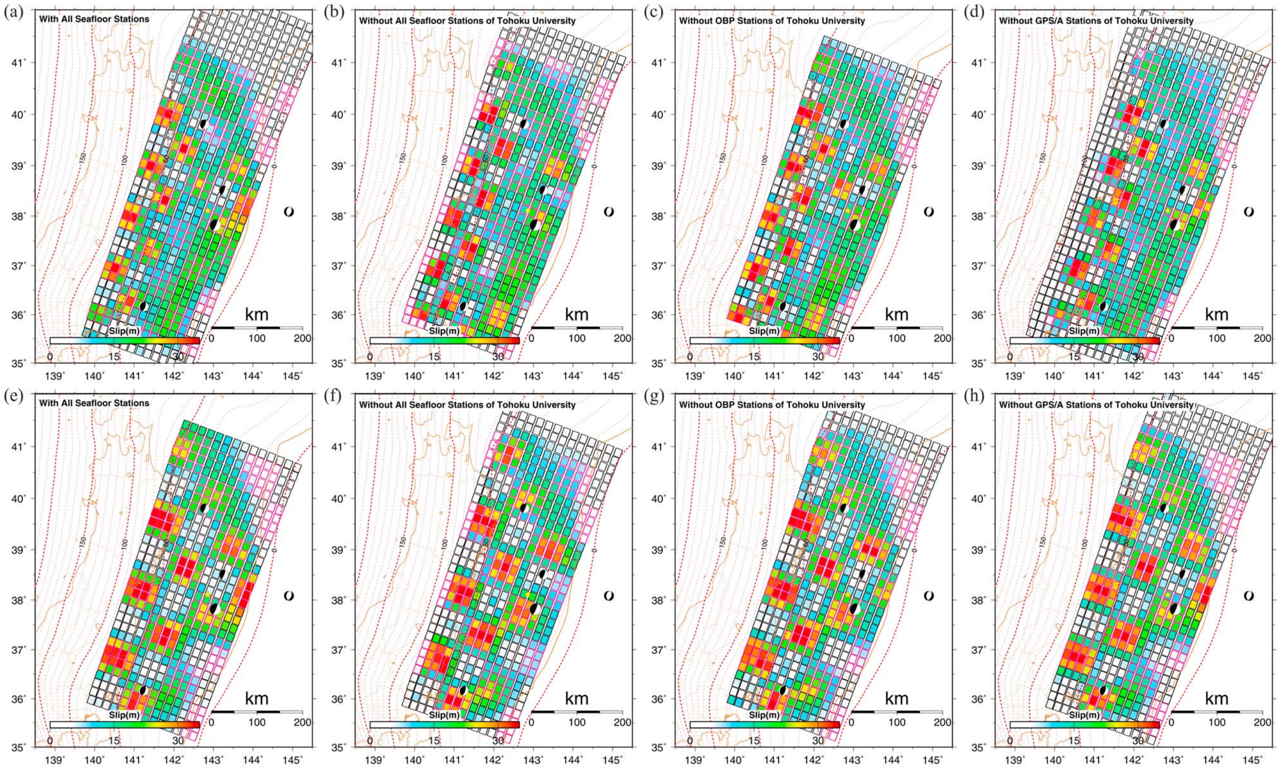

Figure 6. Results of Checkerboard Resolution Tests. Estimated slip distributions from the displacement fields synthesized based on the checkerboard pattern for slip of 30 or 0 m are exhibited. (a–d) The results for the cases in which the square patch size is 60 km parallel and perpendicular to the Japan Trench, (e–h) the cases in which the patch size is 80 km. The subfaults where the slip is distributed are bordered with purple lines. Figures 5a and 5e show the results by using displacements that synthesized for all seafloor stations. Figures 5b and 5f present the results by excluding displacements at seafloor stations that were installed by Tohoku University. Figures 5c and 5g show the results without data from OBP stations of Tohoku University. Figures 5d and 5h exhibit the results without data from Tohoku University's GPS/A stations. Red broken contours indicate the depth of the plate boundary [*Nakajima and Hasegawa*, 2006]. Centroid momentum tensor solutions of the main shock, largest foreshock (M7.3, on 9 March 2011), and large aftershocks that occurred on 11 March 2011 are represented by the beach-ball symbols [*Hirose et al.*, 2011].

by means of the inversion algorithm in the same manner as for the real data in this study. The weights of the constraint conditions, initial value of the each slip component, and the location and number of subfaults are optimized by minimizing ABIC. Random errors representing observational noise are added to the calculated displacements when the displacement field is synthesized. Here, we carried out 8 CRTs with different square checkerboard patch sizes of 60 and 80 km, and with changing the usage of the displacements data at seafloor stations. The results are shown in Figure 6.

[21] The results of the CRTs clarify that the displacements observed at seafloor stations of Tohoku University are essential to resolve the fault slip. Based on the results, slip area along the trench can not be resolved when we do not use the data from our OBP stations (compare Figures 6a and 5d with 5b and 5c, as well as 5e and 5h with 5f and 5g). A comparison of Figures 6a and 5c with 5b and 5d indicates that the downdip limit of the PRA is well constrained when we use the data from our GPS/A stations. Therefore, we conclude that the displacements observed at OBP and GPS/A stations of Tohoku University significantly increase the spatial resolution on the plate interface off Miyagi Prefecture, and the sizes and slip amounts of the PRA and VLSA are accurate enough to discuss the generation and preparation process of the 2011 Tohoku Earthquake.

[22] The second type of computational tests for the spatial resolution is the Reconstruction Tests (RTs). We carried out two RTs to confirm the extent of the slip area at very shallow (≤15 km in depth) portions of the plate interface along the Japan Trench. In the tests the displacement at each observation site is produced by adding the calculated displacement due to different slip amounts of 10, 20 and 50 m at the very shallow portion of the plate interface off Fukushima (RT1) and Iwate Prefectures (RT2) to the observed displacement. The inversion algorithm, in which the weights of the constraint conditions, initial value of the each slip component, and the location and number of subfaults are optimized by minimizing ABIC, is the same as that used for the CRTs. Results of the RTs are shown in Figure 7.

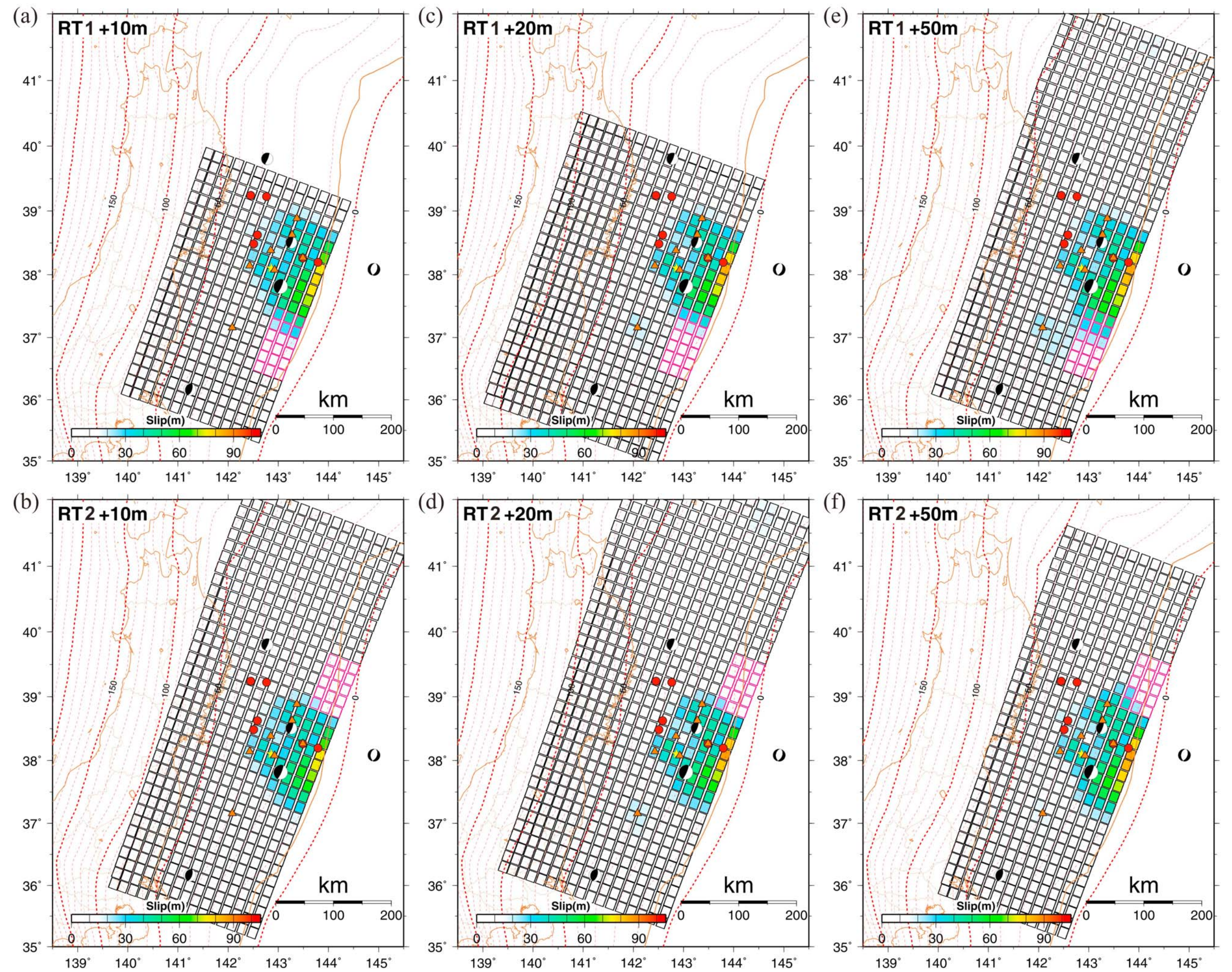

Figure 7. Results of Reconstruction Tests. Estimated coseismic slip distributions based on displacement fields calculated by adding the displacements expected from the assumed slip off Iwate (Figures 6a, 6c, and 6e) and Fukushima Prefecture (Figures 6b, 6d, and 6f) to the original observed data. The assumed slip values used are (a and b) 10, (c and d) 20, and (e and f) 50 m, respectively. The subfaults where the slip is distributed are bordered with purple lines. Red broken contours indicate the depth of the plate boundary [*Nakajima and Hasegawa*, 2006]. Centroid momentum tensor solutions of the main shock, largest foreshock (M7.3, on 9 March 2011), and large aftershocks that occurred on 11 March 2011 are represented by the beach-ball symbols [*Hirose et al.*, 2011]. Red circles and orange triangles point OBP and GPS/A stations.

[23] Based on the RT results, a slip of less than 20 m on the very shallow plate interface off Fukushima Prefecture may not affect the final coseismic slip distribution (Figure 7b), and a slip of more than 20 m may be mistakenly mapped onto the middle portion (around 30 km in depth) of the plate interface (Figures 7d and 7f), which is also the case for the slip on the very shallow plate interface off Iwate Prefecture (Figures 7a, 7c, and 7e).

3.2.2. Examination for the Site Dependency

[24] We produced a modified displacement field data set by excluding some of the 12 seafloor stations, and then estimated the coseismic slip distribution using the same parameters as those used for analysis of the full data set. A total of 4096 (2^{12}) cases were tested, but only 13 cases are described in the Tables 3 and 4, and the Text S1 of the auxiliary material.[1] Table 3 shows the estimated maximum slip, total released moment, and the dimensions of the primary rupture area for large (≥20 m) slip and very large (≥50 m) slip.

[25] Considering the results of these tests, we can conclude that the size of VLSA (≥50 m) along the Japan Trench is not significantly underestimated. The width and length of the VLSA are not greater than 60 km in the trench normal direction and 160 km in the trench parallel direction. This fault is still extremely small for an earthquake of Mw 8.49 [*Fujii and Matsu'ura*, 2000; *Murotani et al.*, 2008].

[1]Auxiliary materials are available in the HTML. doi:10.1029/2012JB009186.

Table 3. Results of Inversion Analyses[a]

			Primary Rupture Area				Area of Very Large Slip			
Case	Maximum Slip (m)	Total Released Moment (10^{22}Nm (Mw))	Width (km)	Length (km)	Released Moment (10^{22}Nm (Mw))	Proportion to the Total Released Moment (%)	Width (km)	Length (km)	Released Moment (10^{22}Nm (Mw))	Proportion to the Total Released Moment (%)
1	86.6	4.40 (9.03)	140	180	2.44 (8.86)	55.5	60	120	7.84 (8.53)	17.8
S1	42.5	3.72 (8.98)	120	280	1.77 (8.77)	47.7	-	-	-	-
S2	54.3	4.11 (9.01)	160	160	2.10 (8.81)	51.1	60	40	2.50 (8.20)	6.1
S3	64.3	4.29 (9.02)	140	180	2.26 (8.84)	52.8	60	100	8.66 (8.56)	20.2
S4	90.8	4.09 (9.01)	140	220	2.06 (8.81)	50.4	40	100	4.91 (8.39)	12.0
S5	49.2	4.00 (9.00)	140	180	2.19 (8.83)	54.7	-	-	-	-
S6	90.7	4.09 (9.01)	140	260	2.18 (8.83)	53.2	40	100	4.84 (8.39)	11.8
S7	64.0	4.15 (9.01)	140	160	2.21 (8.83)	53.3	60	80	7.29 (8.51)	17.6
S8	33.1	3.84 (8.99)	140	240	1.72 (8.76)	44.7	-	-	-	-
S9	86.8	4.06 (9.01)	140	220	2.19 (8.83)	53.8	20	100	4.27 (8.35)	10.5
S10	86.2	4.47 (9.03)	140	180	2.50 (8.87)	56.0	60	120	7.87 (8.53)	17.6
S11	90.9	4.20 (9.02)	140	180	2.06 (8.81)	48.9	40	120	7.21 (8.51)	17.1
S12	86.3	4.33 (9.02)	140	180	2.38 (8.85)	54.9	60	120	7.71 (8.52)	17.8
S13	86.7	4.25 (9.02)	140	180	2.41 (8.85)	56.6	60	120	7.68 (8.52)	18.1

[a]Maximum slip, total released moment, width (in the direction normal to the trench) and length (in the direction parallel to the trench) of the primary rupture area with large (≥20 m) slip and very large (≥50 m) slip, released moment in the primary rupture area and the area of very large slip, and the corresponding fraction of the total released moment are presented. The first column lists the corresponding figure number. The inclusion/exclusion of data from seafloor sites is summarized in Table 2.

3.2.3. Comparison With the Other Studies

[26] Coseismic slip distribution of the 2011 off the Pacific coast of Tohoku earthquake has been investigated by many studies based on seismological, geodetic, and tsunamic data. Several studies have suggested that very large coseismic slip (≥50 m) occurred near the Japan Trench [e.g., *Ito et al.*, 2011a, 2011b; *Lay et al.*, 2011; *Maeda et al.*, 2011; *Shao et al.*, 2011; *Yagi and Fukahata*, 2011]. The maximum slip as 85 m estimated by us is largest value among these studies. Considering estimation error of us and other researches, however, 85 m is not too large, and we conclude that the maximum slip must be larger than 65 m.

[27] *Lay et al.* [2011], *Shao et al.* [2011], and *Yagi and Fukahata* [2011] have used seismic waveform data, and the slip area near the coast in the Miyagi-oki region is also estimated in their results as well as the result of *Ito et al.* [2011a] based on terrestrial GPS and seafloor GPS/A displacements. Tsunami waveform data is applied by *Maeda et al.* [2011] to estimate coseismic slip on 12 rectangular faults, and slip amount on a fault beneath the Miyagi-oki region is estimated as 10 m. As we described previously, the areas that ruptured during the earthquakes off Miyagi Prefecture in 1978 again ruptured during the 2011 Tohoku Earthquake [cf. *Iinuma et al.*, 2011].

[28] With respect to the region off Fukushima Prefecture, which overlaps the rupture areas of past earthquakes, *Ammon et al.* [2011], *Simons et al.* [2011] and *Yagi and Fukahata* [2011] estimated large slip at the region based on seismological data. *Fujii et al.* [2011] also estimated this slipped area off Fukushima Prefecture based on Tsunami waveform data. The rupture areas of earthquakes that occurred in 1938 [*Murotani*, 2003] probably ruptured again during the event in 2011 transmitting short-period seismic waves at the down dip edges of the areas [*Ishii*, 2011; *Koper et al.*, 2011].

Table 4. Data Usage in the Examinations[a]

	Station Code											
Case	GJT3	GJT4	MYGI	MYGW	FUKU	KAMS	KAMN	TJT1	P02	P06	TM1	TM2
1	✓	✓	✓	✓	✓	✓	✓	✓	✓	✓	✓	✓
S1	-	-	-	-	-	-	-	-	-	-	-	-
S2	-	-	✓	✓	✓	✓	✓	✓	✓	✓	✓	✓
S3	✓	✓	✓	✓	✓	✓	✓	-	✓	✓	✓	✓
S4	✓	✓	-	-	-	-	-	✓	✓	✓	✓	✓
S5	-	-	✓	✓	✓	✓	✓	-	-	-	✓	✓
S6	✓	✓	-	-	-	-	-	✓	✓	✓	-	-
S7	✓	✓	✓	✓	✓	✓	✓	-	-	-	-	-
S8	-	-	-	-	-	-	-	✓	✓	✓	✓	✓
S9	✓	✓	-	-	✓	✓	✓	✓	✓	✓	✓	✓
S10	✓	✓	✓	✓	-	✓	✓	✓	✓	✓	✓	✓
S11	✓	✓	✓	✓	✓	-	-	✓	✓	✓	✓	✓
S12	✓	✓	✓	✓	✓	✓	✓	✓	✓	✓	-	-
S13	✓	✓	✓	✓	✓	✓	✓	✓	-	-	✓	✓

[a]Data observed at seafloor sites are included (✓)/excluded (–) in the inversion analyses whose results are presented in the auxiliary material and the main text. The first column lists the corresponding figure number.

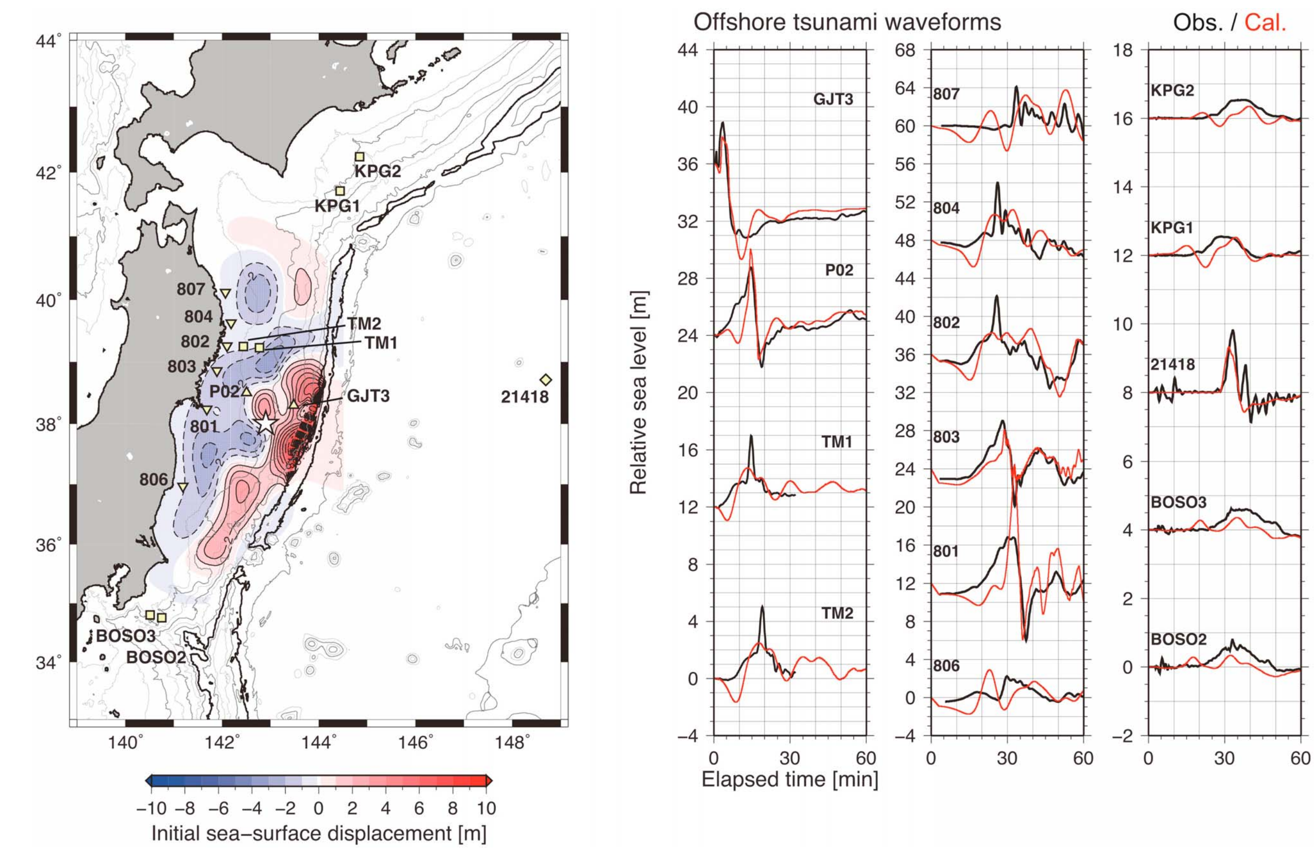

Figure 8. Synthesized tsunami waveform. (left) Distribution of initial sea-surface height estimated from the coseismic slip distribution shown in Figure 3. Star indicates earthquake epicenter. Areas shaded gray are outside the influence area. Contour interval is 1 m. (right) Tsunami calculation results 60 min after the 2011 Tohoku earthquake. Comparison of observed (black lines) and calculated (red lines) waveforms at nine OBP gauges (GJT3, P02, TM1, TM2, KPG2, KPG1, BOSO3, BOSO2 and 21418) and six GPS buoys (807, 804, 802, 803, 801 and 806) are shown.

3.3. Tsunami Waveform

[29] We synthesized tsunami waveforms on the sea surface and at seafloor tsunami observation sites based on the seafloor displacement field calculated from the estimated coseismic interplate slip distribution. The calculations were performed applying the linear long-wave approximation [*Satake*, 1995], and the results are shown in Figure 8, together with measured tsunami waveforms. It can be seen that the calculated and observed waveforms are in general agreement with respect to heights and arrival times.

[30] However, the maximum tsunami heights at sites off Iwate Prefecture (TM1, TM2, 802 and 804) are underestimated. On the other hand, the tsunami heights at near-coastal sites off Miyagi Prefecture are overestimated. This comparison suggests that the displacement and thus the degree of slip off southern Iwate Prefecture may be underestimated. It may be necessary to extend the VLSA to the north in order to explain all tsunami waveforms. Arrival time of first rising tsunami wave observed at site off Fukushima Prefecture (806) is about 5 min faster than the synthesized one, while the height of the calculated waveform is $4 \sim 5$ times larger than the observed one. This implicates that the estimated coseismic slip off Fukushima Prefecture is overestimated with respect to the degree of slip and is wrongly mapped on the plate interface too far from the coast.

[31] To examine the implications described above, we have tested several coseismic slip distribution models by changing slip distributions off Iwate and Fukushima prefectures with trial and error to keep residuals of coseismic displacements not so large. Results of the two cases are shown in Figure 9. In Case 1, coseismic slip distribution in the VLSA and off Iwate prefecture are modified as following procedures; i) an average value of the slip on the shallowest subfaults whose slip are estimated as more than 20 m is calculated, ii) the half of the average slip is assigned 3 subfaults along the Japan Trench, off Iwate prefecture. In Case 2, modified model is constructed as follows; i) an average value of the slip on the shallowest subfaults whose slip are estimated as more than 20 m is calculated as well as Case 1, ii) the half of the average slip is assigned on 4 shallowest subfaults south adjacent to the VLSA, off Fukushima prefecture, and iii) significant slip on the plate interface off Fukushima prefecture around 30 km in depth is cut in half and shifted to the deeper (around 40 km in depth) portion. Modified slip distributions are shown in Figure 9 with displacement residuals and synthesized tsunami waveforms based on the slip distributions.

[32] The agreement of the observed and synthesized tsunami waveform slightly improved, but sharp-peaked high waves are not well synthesized base on the modified slip

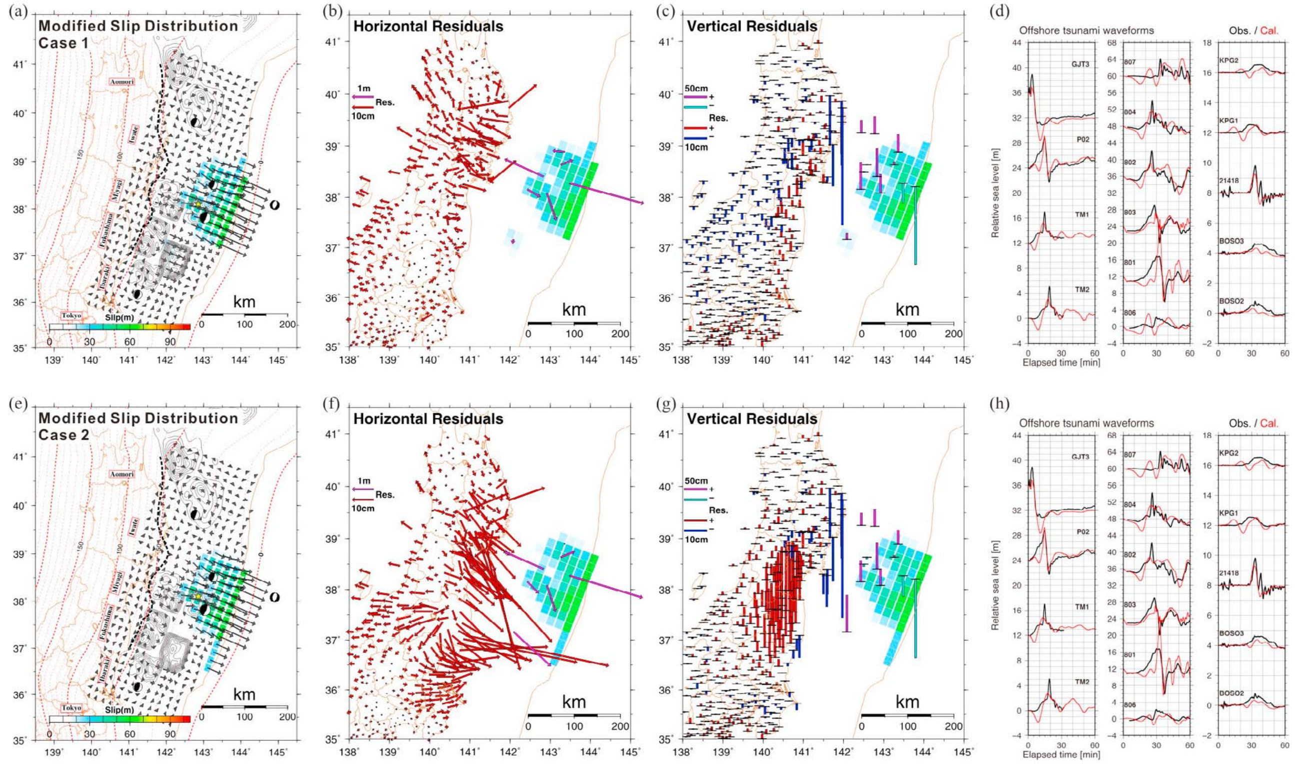

Figure 9. Modified coseismic slip distribution models, the residuals of displacements, and synthesized tsunami waveforms. (a–d) Case 1, (e–h) Case 2. Modified coseismic slip distribution models (Figures 9a and 9e). Symbols same as Figure 3a are drawn in the panels. Horizontal components of the residuals (Figures 9b and 9f). Vertical components of the residuals (Figures 9c and 9g). The residual is determined by subtracting the calculated displacement based on the modified coseismic slip distribution from the observed displacement for each site and case. Synthesized tsunami waveforms estimated from the modified coseismic slip distribution models are exhibited in the same manner as Figure 8 (Figures 9d and 9h).

distribution model in Case 1 (Figure 9d), while both horizontal and vertical components of displacement residuals significantly become larger (Figures 9b and 9c). Especially, horizontal residuals of the sites north of 38.5 degree in latitude are strongly affected even though the modification of the slip distribution is performed with respect to the furthest subfaults from the coastline. In Case 2, disturbance of the displacement residuals are too large to claim that this modified model is good (Figures 9f and 9g), even though the agreement of the tsunami waveform at 806 is significantly improved with the modification (Figure 9h). It is very difficult to find a model that simultaneously satisfies the geodetic and tsunamic data as *Koketsu et al.* [2011] did not used tsunami data for their final joint inversion because of the location difference of the areas of the maximum slip.

[33] The examination and comparison with the tsunami waveform data suggests that very large slip occurred only on the very shallow ($\leq$15 km) portion of the plate interface along the Japan Trench, and the width of the VLSA is well constrained by using not terrestrial but only seafloor geodetic data. Regardless, the comparison between the observed and calculated tsunami waveforms does not require large slip on the very shallow portion of the plate interface off Fukushima Prefecture. Figure 5 shows the relationships between rupture areas, seismic moments, average slips and combined areas of asperities with respect to the modified coseismic slip models (black circles partially hidden under the white star). It shows that modified models do not significantly differ from the original estimation. Therefore, it is indisputable that an extremely large amount of slip occurred within a very small area near the Japan Trench off not Fukushima or Iwate Prefectures but Miyagi Prefecture, which breaks the conventional scaling law concerning interplate earthquakes in the subduction zone around the Japanese Islands.

3.4. Seismic Cycle

[34] If the 2011 off the Pacific coast of Tohoku Earthquake completely released the stress in the VLSA that had been accumulated since the previous earthquake broken the area, we can expect that the coseismic slip balances the slip deficit accumulated during the interseismic period. *Hasegawa et al.* [2011] investigated the stress field near the fault plane of the main shock and suggested that the background deviatoric stress which caused the 2011 earthquake is mostly released. Taking stress release due to the aseismic slip events and inelastic deformation such as viscoelastic relaxation into account, we assume a relationship between changes in the stress as,

$$\Delta\sigma^{coseismic} = \Delta\sigma^{interseismic} - \Delta\sigma^{aseismic} - \Delta\sigma^{inelastic}, \quad (1)$$

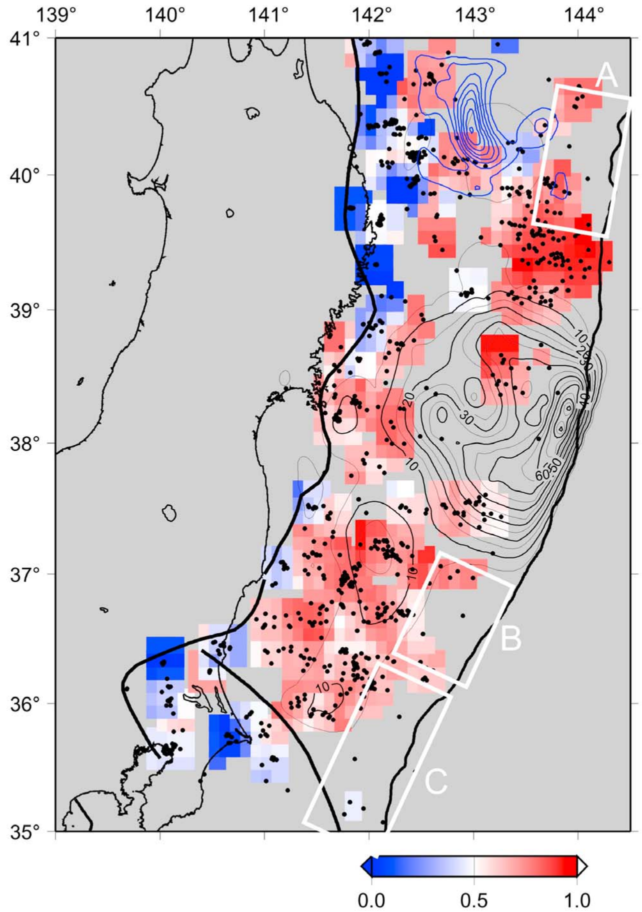

Figure 10. Comparison between coseismic slip distribution and interplate coupling coefficient distribution deduced by *Uchida and Matsuzawa* [2011]. Interplate coupling coefficient estimated from small repeating earthquakes for the period from 1993 to March 2007 (color). Distribution of small repeating earthquakes (black dots) and coseismic slip area are also shown in this figure. Bold lines denote the down-dip limit of interplate earthquakes [*Igarashi et al.*, 2001; *Uchida et al.*, 2009] and the trench axis. Northeastern limit of the Philippine Sea plate is also denoted by a bold line. The average coupling coefficient is estimated for each 0.3 degree by 0.3 degree window that has three or fewer repeating earthquake groups.

where $\Delta\sigma^{coseismic}$, $\Delta\sigma^{interseismic}$, $\Delta\sigma^{aseismic}$ and $\Delta\sigma^{inelastic}$ stand for changes in the stress due to the main shock coseismic slip, interseismic plate coupling, aseismic slip events on the plate interface and inelastic relaxation processes. Therefore, we can estimate interseismic slip deficit based on the coseismic slip distribution at the minimum, because elastic deformation due to the interseismic plate coupling balances or exceeds the coseismic elastic deformation. The estimated maximum slip associated with the 2011 Tohoku Earthquake is about 85 m. If we assume that the interplate coupling between the subducting Pacific plate and the continental plate during the interseismic period is 100% in the VLSA, then the earthquake recurrence interval is about 1000 $\sim$ 1200 years, since the plate convergence rate in this area is 70 $\sim$ 85 mm/year [*Altamimi et al.*, 2007]. This estimation may be an upper bound of the recurrence interval, and is consistent with the idea that the Jogan Earthquake in 869 [*Minoura et al.*, 2001; *Sawai et al.*, 2008], not the Keicho Earthquake in 1611 [*Sawai et al.*, 2008], represents the preceding event in the series that includes the 2011 Tohoku Earthquake. 400 years since Keicho Earthquake is too short even if the maximum slip is overestimated by about 25 m.

[35] *Uchida and Matsuzawa* [2011] estimated the interplate coupling coefficient before the Tohoku Earthquake in 2011 around the source region of the earthquake based on an analysis of small repeating earthquakes. They suggested that shallow (≥30 km in depth) areas of the plate interface where no such activity exists may be 100% coupled. We therefore compared our coseismic slip distribution model with their coupling coefficient distribution, and the results are shown in Figure 10. It can be seen that the VLSA is almost coincident with the area where no repeating earthquakes have occurred. The northern edge of this area corresponds to the southern edge of the area with strong, but not full, interplate coupling off Iwate Prefecture. This suggests that the area with partial coupling has different frictional properties to those of adjacent areas to the south and north, so that the former area acted as a barrier to northward rupture propagation during the 2011 Tohoku Earthquake.

[36] Analysis of small repeating earthquake activity suggests that the interplate coupling rates in areas with no such activity are either 0 or 100%, and such activity does not occur at the most shallow portions of the plate interface, namely not only the VLSA but also regions A, B and C in Figure 10. If the interplate coupling rates in these areas are 100%, such coupled zones may rupture in the same manner as the 2011 event and generate huge tsunamis. Thus, the question then arises as to whether 100% coupling at such shallow portions of the interface during the interseismic period could be detected by analyzing terrestrial GPS data. To this end, we calculated the expected velocity fields on the homogeneous elastic half-space based on the assumed interplate coupling in the regions A, B and C, and the results are shown in Figure 11. Water depth of the seafloor is taken into account in these calculations as same as the inversion analysis (see section 2.2). The velocities at the terrestrial GPS stations are smaller than 2 mm/year that is the lower limit to detect by the continuous GPS observations. Displacements due to interplate coupling at other portions of the plate interface, co- and post-seismic deformation associated with inland earthquakes, and observational noise prevent us from isolating the effect of interplate coupling in the area along the trench. However, the displacement rates on the seafloor are large enough to be detected, namely larger than

Figure 11. Expected velocity fields due to interplate coupling at the very shallow portion of the plate interface. Horizontal (Figures 11a, 11c, and 11e) and vertical (Figures 11b, 11d, and 11f) displacements due to the assumed slip deficit at the very shallow portion of the plate interface are shown by colored contours. The subfaults where interplate coupling rates are assumed as 100% are exhibited colored squares. The areas where the full coupling are assumed to correspond to (a and b) region A, (c and d) region B, and (e and f) region C shown in Figure 10.

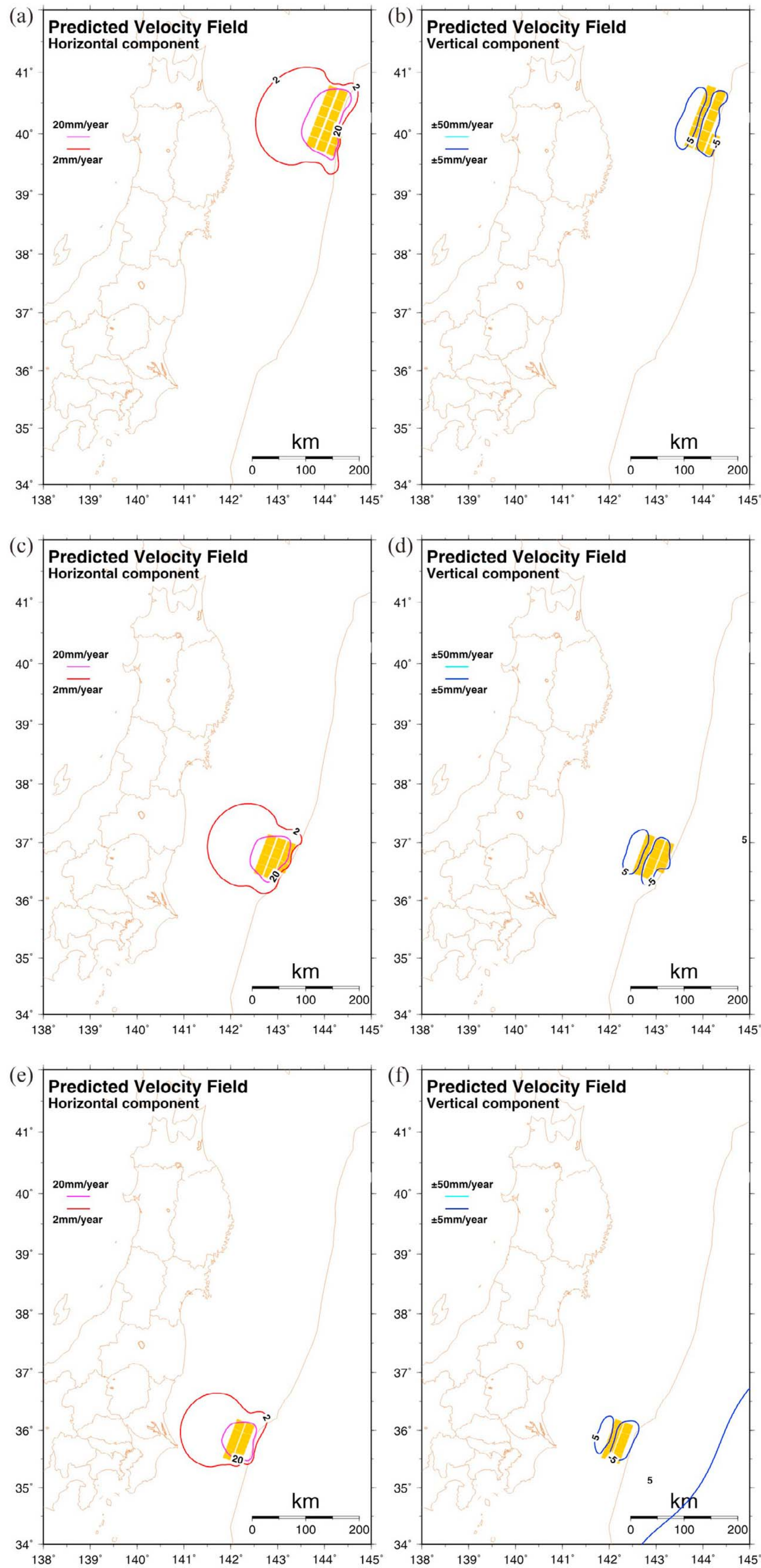
(a)
Predicted Velocity Field
Horizontal component
20mm/year
2mm/year
(b)
Predicted Velocity Field
Vertical component
±50mm/year
±5mm/year
(c)
Predicted Velocity Field
Horizontal component
20mm/year
2mm/year
(d)
Predicted Velocity Field
Vertical component
±50mm/year
±5mm/year
(e)
Predicted Velocity Field
Horizontal component
20mm/year
2mm/year
(f)
Predicted Velocity Field
Vertical component
±50mm/year
±5mm/year
km
0 100 200

Figure 11

20 mm/year, around the coupling zones. Therefore, it is essential to improve the seafloor geodetic observation network. This involves enhancing both the density and the sensitivity of the network in order to assess the seismic risk due to interplate coupling at very shallow portions of the plate interface beneath the northeastern Japanese Islands.

4. Summary

[37] We estimated coseismic slip distribution of the 2011 off the Pacific Coast of Tohoku Earthquake based on the displacements at terrestrial and seafloor geodetic stations by means of an inversion method. Estimated coseismic slip distribution can be generally divided into three different areas; 1) The primary rupture area with the area of very large (≥50 m) slip along the Japan Trench, 2) The plate interface off Fukushima Prefecture in the intermediate depth, 3) The area near the coast of Miyagi Prefecture where M $\sim$ 7.5 earthquakes have repeatedly occurred. Both the primary rupture area and the area of very large slip released too large moment for their lengths and widths breaking the scaling laws previously deduced. Calculated tsunami waveforms based on the estimated coseismic slip distribution mostly correspond with the observed ones. Estimated maximum slip in the area of very large slip reaches about 85 m near the Japan Trench suggesting that the 2011 Tohoku Earthquake released strain energy that had accumulated over the past 1000 years, probably since the Jogan Earthquake in 869. Accurate assessments of seismic risks on very shallow plate interfaces in subduction zones throughout the world can be obtained by improving the quality and quantity of seafloor geodetic observations.

Appendix A: Detail of the Inversion Method

[38] We used an inversion method proposed by *Iinuma* [2009], which revised the inversion method devised by *Yabuki and Matsu'ura* [1992] and *Matsu'ura et al.* [2007]. The method incorporates two constraint conditions other than the smoothing constraint into the prior probability density function (PDF). Damping to initial values and the Dirichlet type boundary condition are adopted. All constraint conditions are represented as

$$\mathbf{La} = 0, \tag{A1}$$

$$\mathbf{Ia} = \mathbf{a}_0, \tag{A2}$$

$$\mathbf{Ba} = \mathbf{b}, \tag{A3}$$

where $\mathbf{L}$ is a discrete version of the Laplacian operator matrix [*Fukuda and Johnson*, 2008]. $\mathbf{I}$ is an $M \times M$-dimensional unit matrix where M is the dimension of the model parameter vector, $\mathbf{a}$, and $\mathbf{a}_0$ is an initial value vector. Using $\mathbf{a}_0(\geq 0)$ prevents all of the components of the solution of $\mathbf{a}$ from becoming negative. $\mathbf{a}$ is a parameter vector defined as,

$$\mathbf{a}^{\mathrm{T}} = [a_{11}, \cdots, a_{1K}, a_{21}, \cdots, a_{2K}] \tag{A4}$$

where a_{jk} are expansion coefficients of u_j for the k-th basis function, u_j is the j-th component of the slip or slip deficit on the fault surface S. Here, boxcar basis functions are used to express the boundary condition explicitly. $\mathbf{B}$ and $\mathbf{b}$ are defined as

$$\mathrm{B}_{kl} = \begin{cases} \delta_{kl} & k(l)\text{-th basis function corresponds to the boundary node,} \\ 0 & \text{otherwise,} \end{cases} \tag{A5}$$

$$\mathrm{b}_k = \begin{cases} b & k\text{-th basis function corresponds to the boundary node,} \\ 0 & \text{otherwise.} \end{cases} \tag{A6}$$

Here, b is the boundary value that the model parameter should take on the edge of the modeled fault. Different boundary conditions can be used on edges of the modeled fault by changing B_{kl} and b_k. For the case of this study about the 2011 Tohoku earthquake, we imposed the boundary constraint on the north, south and bottom edges of a plate boundary fault by changing B_{kl} as

$$\mathrm{B}_{kl} = \begin{cases} \delta_{kl} & k(l)\text{-th basis function corresponds to north, south or bottom boundary node,} \\ 0 & \text{otherwise,} \end{cases} \tag{A7}$$

when estimating the back slip distribution. Here, $\mathbf{a}_0$ and b can be determined based on ABIC. In present study, two constants $a_{0,1}$ and $a_{0,2}$ are utilized as initial values of a_{1k} and a_{2k} for $k = 1, \cdots, K$, and the value of $a_{0,1}$ and $a_{0,2}$ are optimized by minimizing ABIC. b is assumed to be as 0.

[39] The evaluation function, F, is defined as

$$F = \beta_1^{-2}\mathbf{a}^{\mathrm{T}}\mathbf{L}^{\mathrm{T}}\mathbf{La} + \beta_2^{-2}(\mathbf{a}-\mathbf{a}_0)^{\mathrm{T}}(\mathbf{a}-\mathbf{a}_0) + \beta_3^{-2}(\mathbf{Ba}-\mathbf{b})^{\mathrm{T}}(\mathbf{Ba}-\mathbf{b}) \tag{A8}$$

$$= \left\| \begin{bmatrix} \beta_1^{-1}\mathbf{L} \\ \beta_2^{-1}\mathbf{I} \\ \beta_3^{-1}\mathbf{B} \end{bmatrix} \mathbf{a} - \begin{bmatrix} \beta_1^{-1}0 \\ \beta_2^{-1}\mathbf{a}_0 \\ \beta_3^{-1}\mathbf{b} \end{bmatrix} \right\|^2 \tag{A9}$$

$$= |\mathbf{Aa} - \alpha|^2, \tag{A10}$$

where β_i^2 is an unknown weight factor for each constraint condition, and

$$\mathbf{A} = \begin{bmatrix} \beta_1^{-1}\mathbf{L} \\ \beta_2^{-1}\mathbf{I} \\ \beta_3^{-1}\mathbf{B} \end{bmatrix}, \tag{A11}$$

$$\alpha = \begin{bmatrix} \beta_1^{-1}0 \\ \beta_2^{-1}\mathbf{a}_0 \\ \beta_3^{-1}\mathbf{b} \end{bmatrix}. \tag{A12}$$

Using $\mathbf{a}'$ defined as $\mathbf{a}' = \mathbf{A}^{-g}\alpha$, where $\mathbf{A}^{-g}$ indicates the generalized inverse matrix of $\mathbf{A}$, F is rewritten as

$$F = (\mathbf{a} - \mathbf{a}')^{\mathrm{T}}\mathbf{A}^{\mathrm{T}}\mathbf{A}(\mathbf{a} - \mathbf{a}'). \tag{A13}$$

A prior PDF is defined using this function, as follows

$$p\left(\mathbf{a};\beta_1^2,\beta_2^2,\beta_3^2\right) = (2\pi)^{-M/2}\,\|\mathbf{A}^{\mathrm{T}}\mathbf{A}\|^{1/2} \cdot \exp\left[-(\mathbf{a} - \mathbf{a}')^{\mathrm{T}}\mathbf{A}^{\mathrm{T}}\mathbf{A}(\mathbf{a} - \mathbf{a}')/2\right]. \tag{A14}$$

The prior PDF is maximized by minimizing the evaluate function, F.

[40] The posterior PDF can be determined by incorporating this prior PDF and the conditional PDF of the data as,

$$p(\mathbf{d}|\mathbf{a};\sigma^2) = \left(2\pi\sigma^2\right)^{-N/2}\,\|\mathbf{E}\|^{-1/2} \cdot \exp\left[-(\mathbf{d} - \mathbf{H}\mathbf{a})^{\mathrm{T}}\mathbf{E}^{-1}(\mathbf{d} - \mathbf{H}\mathbf{a})/2\sigma^2\right]. \tag{A15}$$

Here, $\mathbf{H}$ is an $N \times M$-dimensional coefficient matrix that connects the N-dimensional data vector, $\mathbf{d}$, and the M-dimensional model parameter vector, $\mathbf{a}$, and the error vector, $\mathbf{e}$, is assumed to be Gaussian with zero mean and covariance $\sigma^2\mathbf{E}$.

[41] The posterior PDF is given as follows

$$p\left(\mathbf{a};\beta_1^2,\beta_2^2,\beta_3^2|\mathbf{d}\right) = c_4\left(2\pi\sigma^2\right)^{-N/2}(2\pi)^{-M/2}\,\|\mathbf{E}\|^{-1/2}\,\|\mathbf{A}^{\mathrm{T}}\mathbf{A}\|^{1/2} \cdot \exp\left[-s(\mathbf{a})/2\sigma^2\right], \tag{A16}$$

with

$$s(\mathbf{a}) = (\mathbf{d} - \mathbf{H}\mathbf{a})^{\mathrm{T}}\mathbf{E}^{-1}(\mathbf{d} - \mathbf{H}\mathbf{a}) + (\mathbf{a} - \mathbf{a}')^{\mathrm{T}}\mathbf{A}'^{\mathrm{T}}\mathbf{A}'(\mathbf{a} - \mathbf{a}'), \tag{A17}$$

where

$$\mathbf{A}' = \sigma\mathbf{A} \tag{A18}$$

$$= \begin{bmatrix} \rho_1\mathbf{L} \\ \rho_2\mathbf{I} \\ \rho_3\mathbf{B} \end{bmatrix}, \tag{A19}$$

with $\rho_k = \sigma/\beta_k$, and c_4 is a normalizing factor that is equivalent to the inverse of the marginal likelihood, $L_3(\sigma^2,\ \rho_1^2,\ \rho_2^2,\ \rho_3^2)$.

[42] For any solution that minimizes $s(\mathbf{a})$, the variation of $s(\mathbf{a})$ with respect to $\mathbf{a}$ must vanish. Thus, we obtain a fundamental equation to be satisfied by the solution $\mathbf{a}^*$ from $\left(\partial s(\mathbf{a})/\partial\mathbf{a}|_{\mathbf{a}=\mathbf{a}^*}\right) = 0$:

$$\mathbf{H}^{\mathrm{T}}\mathbf{E}^{-1}(\mathbf{d} - \mathbf{H}\mathbf{a}^*) + \mathbf{A}'^{\mathrm{T}}\mathbf{A}'(\mathbf{a}' - \mathbf{a}^*) = 0 \tag{A20}$$

$$\mathbf{H}^{\mathrm{T}}\mathbf{E}^{-1}\mathbf{d} + \rho_2^2\mathbf{a}_0 + \rho_3^2\mathbf{B}^{\mathrm{T}}\mathbf{b} = \mathbf{H}^{\mathrm{T}}\mathbf{E}^{-1}\mathbf{H}\mathbf{a}^* + \rho_1^2\mathbf{L}^{\mathrm{T}}\mathbf{L}\mathbf{a}^* + \rho_2^2\mathbf{a}^* + \rho_3^2\mathbf{B}^{\mathrm{T}}\mathbf{B}\mathbf{a}^* \tag{A21}$$

Thus, we obtain the solution of $\mathbf{a}$ as

$$\mathbf{a}^* = \left(\mathbf{H}^{\mathrm{T}}\mathbf{E}^{-1}\mathbf{H} + \rho_1^2\mathbf{L}^{\mathrm{T}}\mathbf{L} + \rho_2^2\mathbf{I} + \rho_3^2\mathbf{B}^{\mathrm{T}}\mathbf{B}\right)^{-1} \cdot \left(\mathbf{H}^{\mathrm{T}}\mathbf{E}^{-1}\mathbf{d} + \rho_2^2\mathbf{a}_0 + \rho_3^2\mathbf{B}^{\mathrm{T}}\mathbf{b}\right). \tag{A22}$$

[43] Now, the marginal likelihood of the hyperparameters is given as follows

$$L_3\left(\sigma^2,\rho_1^2,\rho_2^2,\rho_3^2\right) = \int \left(2\pi\sigma^2\right)^{-N/2}(2\pi)^{-M/2}\,\|\mathbf{E}\|^{-1/2}\,\|\mathbf{A}^{\mathrm{T}}\mathbf{A}\|^{1/2} \cdot \exp\left[-s(\mathbf{a})/2\sigma^2\right]\mathrm{d}\mathbf{a} \tag{A23}$$

$$= \left(2\pi\sigma^2\right)^{-N/2}(2\pi)^{-M/2}\,\|\mathbf{E}\|^{-1/2}\,\|\mathbf{A}^{\mathrm{T}}\mathbf{A}\|^{1/2}\exp\left[-s(\mathbf{a}^*)/2\sigma^2\right] \times \int \exp\left[-(\mathbf{a} - \mathbf{a}^*)^{\mathrm{T}}\left(\mathbf{H}^{\mathrm{T}}\mathbf{E}^{-1}\mathbf{H} + \rho_1^2\mathbf{L}^{\mathrm{T}}\mathbf{L} + \rho_2^2\mathbf{I} + \rho_3^2\mathbf{B}^{\mathrm{T}}\mathbf{B}\right)(\mathbf{a} - \mathbf{a}^*)/2\sigma^2\right]\mathrm{d}\mathbf{a} \tag{A24}$$

$$= \left(2\pi\sigma^2\right)^{-N/2}(2\pi)^{-M/2}\,\|\mathbf{E}\|^{-1/2}\,\|\mathbf{A}^{\mathrm{T}}\mathbf{A}\|^{1/2}\exp\left[-s(\mathbf{a}^*)/2\sigma^2\right] \times \left(2\pi\sigma^2\right)^{M/2}\,\|\mathbf{H}^{\mathrm{T}}\mathbf{E}^{-1}\mathbf{H} + \rho_1^2\mathbf{L}^{\mathrm{T}}\mathbf{L} + \rho_2^2\mathbf{I} + \rho_3^2\mathbf{B}^{\mathrm{T}}\mathbf{B}\|^{-1/2}. \tag{A25}$$

Here, the relationship between $s(\mathbf{a})$ and $s(\mathbf{a}^*)$ is used to obtain

$$s(\mathbf{a}) = s(\mathbf{a}^*) + (\mathbf{a} - \mathbf{a}^*)^{\mathrm{T}}\left(\mathbf{H}^{\mathrm{T}}\mathbf{E}^{-1}\mathbf{H} + \rho_1^2\mathbf{L}^{\mathrm{T}}\mathbf{L} + \rho_2^2\mathbf{I} + \rho_3^2\mathbf{B}^{\mathrm{T}}\mathbf{B}\right) \cdot (\mathbf{a} - \mathbf{a}^*). \tag{A26}$$

[44] We can eliminate σ^2 in equation (A25) by solving the equation such that $\partial L_3/\partial\sigma^2 = 0$, which is the necessary condition for the maximum of the marginal likelihood. We obtain $\sigma^2 = s(\mathbf{a}^*)/N$. Finally, ABIC is written as

$$\begin{aligned}\mathrm{ABIC} &= -2\log L_3\left(\sigma^2,\rho^2\right) + 2K \\ &= (N + M)\log 2\pi + N - N\log N + \log\|\mathbf{E}\| \\ &\quad + N\log s(\mathbf{a}^*) - \log\|\rho_1^2\mathbf{L}^{\mathrm{T}}\mathbf{L} + \rho_2^2\mathbf{I} + \rho_3^2\mathbf{B}^{\mathrm{T}}\mathbf{B}\| \\ &\quad + \log\|\mathbf{H}^{\mathrm{T}}\mathbf{E}^{-1}\mathbf{H} + \rho_1^2\mathbf{L}^{\mathrm{T}}\mathbf{L} + \rho_2^2\mathbf{I} + \rho_3^2\mathbf{B}^{\mathrm{T}}\mathbf{B}\| + 2K\end{aligned} \tag{A27}$$

where K is the number of hyperparameters. Finding the combination of hyperparameters, ρ_1^2, ρ_2^2, and ρ_3^2 that minimizes ABIC is the conclusive problem. We can find the best combination of these hyperparameters using a grid search algorithm.

[45] **Acknowledgments.** We thank the Miyagi Prefectural government for providing us with helicopter flights to collect GPS data from Kinkasan and Enoshima islands. Some GPS data were provided by a research project conducted by the Japan Nuclear Energy Safety Organization to develop evaluation techniques for seismogenic faults. We thank the Geospatial Information Authority of Japan, the Earthquake Research Institute at the University of Tokyo, the Japan Meteorological Agency, the Japan Agency of Marine-Earth Science and Technology, and the National Oceanic and Atmospheric Administration for providing GPS data and tsunami data recorded by cabled ocean-bottom pressure sensors. We are grateful to the Ministry of Land, Infrastructure Transport and Tourism, and the Port and Airport Research Institute for providing tsunami data from GPS buoys. The study was supported by the MEXT project, "Evaluation and disaster prevention research for the coming Tokai, Tonankai and Nankai earthquakes" and JSPS KAKENHI (20244070). Paul Segall and an anonymous reviewer provided thoughtful comments, which improved the manuscript. N. Uchida kindly provided us with coupling coefficient distribution data for the 2011 Tohoku earthquake. Figures were drawn using GMT software [*Wessel and Smith*, 1998].

References

Akaike, H. (1977), On entropy maximization principle, in *Application of Statistics*, edited by P. R. Krishnaiah, pp. 27–41, North-Holland, Amsterdam.

Akaike, H. (1980), Likelihood and the Bayes procedure, in *Bayesian Statistics*, edited by J. M. Bernardo et al., pp. 143–166, Valencia Univ. Press, Valencia, Spain.

Altamimi, Z., X. Collilieux, J. Legrand, B. Garayt, and C. Boucher (2007), ITRF2005: A new release of the International Terrestrial Reference Frame based on time series of station positions and Earth Orientation Parameters, *J. Geophys. Res.*, *112*, B09401, doi:10.1029/2007JB004949.

Ammon, C. J., T. Lay, H. Kanamori, and M. Cleveland (2011), A rupture model of the 2011 off the Pacific coast of Tohoku Earthquake, *Earth Planets Space*, *63*(7), 693–696, doi:10.5047/eps.2011.05.015.

Dach, R., U. Hugentobler, P. Fridez, and M. Meindl (2007), *User Manual of the Bernese GPS Software Version 5.0*, 612 pp., Astron. Inst., Univ. of Bern, Bern.

Fujii, Y., and M. Matsu'ura (2000), Regional difference in scaling laws for large earthquakes and its tectonic implication, *Pure Appl. Geophys.*, *157*(11–12), 2283–2301, doi:10.1007/PL00001085.

Fujii, Y., K. Satake, S. Sakai, M. Shinohara, and T. Kanazawa (2011), Tsunami source of the 2011 off the Pacific coast of Tohoku earthquake, *Earth Planets Space*, *63*(7), 815–820, doi:10.5047/eps.2011.06.010.

Fukuda, J., and K. M. Johnson (2008), A fully Bayesian inversion for spatial distribution of fault slip with objective smoothing, *Bull. Seismol. Soc. Am.*, *98*(3), 1128–1146, doi:10.1785/0120070194.

Hasegawa, A., K. Yoshida, and T. Okada (2011), Nearly complete stress drop in the 2011 Mw 9.0 off the Pacific coast of Tohoku earthquake, *Earth Planets Space*, *63*, 703–707, doi:10.5047/eps.2011.06.007.

Hino, R., Y. Ito, K. Suzuki, S. Suzuki, D. Inazu, T. Iinuma, Y. Ohta, H. Fujimoto, M. Shinohara, and Y. Kaneda (2011), Foreshocks and mainshock of the 2011 Tohoku Earthquake observed by Ocean Bottom Seismic/Geodetic monitoring, Abstract U51B-0008 presented at 2011 Fall Meeting, AGU, San Francisco, Calif., 5–9 Dec.

Hirose, F., K. Miyaoka, N. Hayashimoto, T. Yamazaki, and M. Nakamura (2011), Outline of the 2011 off the Pacific coast of Tohoku earthquake (M_w 9.0)—Seismicity: Foreshocks, mainshock, aftershocks, and induced activity, *Earth Planets Space*, *63*(7), 513–518, doi:10.5047/eps.2011.05.019.

Ide, S., A. Baltay, and G. C. Beroza (2011), Shallow dynamic overshoot and energetic deep rupture in the 2011 Mw 9.0 Tohoku-Oki earthquake, *Science*, *332*(6036), 1426–1429, doi:10.1126/sciene.1207020.

Igarashi, T., T. Matsuzawa, N. Umino, and A. Hasegawa (2001), Spatial distribution of focal mechanisms for interplate and intraplate earthquake associated with the subducting Pacific plate beneath the northeastern Japan arc: A triple-planed deep seismic zone, *J. Geophys. Res.*, *106*(B2), 2177–2191, doi:10.1029/2000JB900386.

Iinuma, T. (2009), Discussion on the rank deficiency of the representation matrix of the smoothing constraint in inversion methods using a Bayesian information criterion, *J. Geod. Soc. Jpn.*, *55*(4), 345–353.

Iinuma, T., M. Ohzono, Y. Ohta, and S. Miura (2011), Coseismic slip distribution of the 2011 off the Pacific coast of Tohoku earthquake (M 9.0) estimated based on GPS data—Was the asperity in Miyagi-oki ruptured?, *Earth Planets Space*, *63*(7), 643–648, doi:10.5047/eps.2011.06.013.

Ishii, M. (2011), High-frequency rupture properties of the M_w 9.0 off the Pacific coast of Tohoku earthquake, *Earth Planets Space*, *63*(7), 609–614, doi:10.5047/eps.2011.07.009.

Ito, A., G. Fujie, S. Miura, S. Kodaira, Y. Kaneda, and R. Hino (2005), Bending of the subducting oceanic plate and its implication for rupture propagation of large interplate earthquakes off Miyagi, Japan, in the Japan Trench subduction zone, *Geophys. Res. Lett.*, *32*, L05310, doi:10.1029/2004GL022307.

Ito, T., K. Ozawa, T. Watanabe, and T. Sagiya (2011a), Slip distribution of the 2011 off the Pacific coast of Tohoku earthquake inferred from geodetic data, *Earth Planets Space*, *63*(7), 627–630, doi:10.5047/eps.2011.06.023.

Ito, Y., T. Tsuji, Y. Osada, M. Kido, D. Inazu, Y. Hayashi, H. Tsushima, R. Hino, and H. Fujimoto (2011b), Frontal wedge deformation near the source region of the 2011 Tohoku-Oki earthquake, *Geophys. Res. Lett.*, *38*, L00G05, doi:10.1029/2011GL048355.

Kido, M., Y. Osada, H. Fujimoto, R. Hino, and Y. Ito (2011), Trench-normal variation in observed seafloor displacements associated with the 2011 Tohoku-Oki earthquake, *Geophys. Res. Lett.*, *38*, L24303, doi:10.1029/2011GL050057.

Koketsu, K., et al. (2011), A unified source model for the 2011 Tohoku earthquake, *Earth Planet. Sci. Lett.*, *310*, 480–487, doi:10.1016/j.epsl.2011.09.009.

Koper, K. D., A. R. Hutko, T. Lay, C. J. Ammon, and H. Kanamori (2011), Frequency-dependent rupture process of the 2011 M_w 9.0 Tohoku earthquake: Comparison of short-period *P* wave backprojection images and broadband seismic rupture models, *Earth Planets Space*, *63*(7), 599–602, doi:10.5047/eps.2011.05.026.

Lay, T., C. J. Ammon, H. Kanamori, L. Xue, and M. J. Kim (2011), Possible large near-trench slip during the 2011 M_w 9.0 off the Pacific coast of Tohoku earthquake, *Earth Planets Space*, *63*(7), 687–692, doi:10.5047/eps.2011.05.033.

Maeda, T., T. Furumura, S. Sakai, and M. Shinohara (2011), Significant tsunami observed at the ocean-bottom pressure gauges during the 2011 off the Pacific coast of Tohoku earthquake, *Earth Planets Space*, *63*(7), 803–808, doi:10.5047/eps.2011.06.005.

Matsu'ura, M., A. Noda, and Y. Fukahata (2007), Geodetic data inversion based on Bayesian formulation with direct and indirect prior information, *Geophys. J. Int.*, *171*(3), 1342–1351.

Minoura, K., F. Imamura, D. Sugawara, Y. Kono, and T. Iwashita (2001), The 869 Jogan tsunami deposit and recurrence interval of large-scale tsunami on the Pacific coast of northeast Japan, *J. Nat. Disaster Sci.*, *23*, 83–88.

Mitsui, Y., and Y. Iio (2011), How did the 2011 off the Pacific coast of Tohoku earthquake start and grow? The role of a conditionally stable area, *Earth Planets Space*, *63*, 755–759, doi:10.5047/eps.2011.05.007.

Miura, S., K. Tachibana, K. Hashimoto, E. Murakami, T. Kono, K. Nida, T. Sato, and S. Hori (1993), GPS observation for regional crustal deformation around the northeastern Japan arc [in Japanese with English abstract], *J. Geod. Soc. Jpn.*, *39*(2), 167–178.

Miyazaki, S., and Y. Hatanaka (1998), The outlines of the GEONET [in Japanese], *Meteorol. Res. Note*, *192*, 105–131.

Murotani, S. (2003), Rupture processes of large Fukushima-Oki earthquakes in 1938, MSc thesis, Univ. of Tokyo, Tokyo.

Murotani, S., H. Miyake, and K. Koketsu (2008), Scaling of characterized slip models for plate-boundary earthquakes, *Earth Planets Space*, *60*(9), 987–991.

Nakajima, J., and A. Hasegawa (2006), Anomalous low-velocity zone and linear alignment of seismicity along it in the subducted Pacific slab beneath Kanto, Japan: Reactivation of subducted fracture zone?, *Geophys. Res. Lett.*, *33*, L16309, doi:10.1029/2006GL026773.

Nakajima, J., T. Matsuzawa, A. Hasegawa, and D. Zhao (2001), Three-dimensionasl tructure of Vp, Vs, and Vp/Vs beneath northeastern Japan: Implications for arc magmatism and fluids, *J. Geophys. Res.*, *106*(B10), 21,843–21,857, doi:10.1029/2000JB000008.

Ohzono, M., Y. Yabe, T. Iinuma, Y. Ohta, S. Miura, K. Tachibana, T. Sato, and T. Demachi (2012), Strain anomalies induced by the 2011 Tohoku earthquake (Mw9.0) as observed by a dense GNSS network in northeastern Japan, *Earth Planets Space*, doi:10.5047/eps.2012.05.015, in press.

Ozawa, S., T. Nishimura, H. Suito, T. Kobayashi, M. Tobita, and T. Imakiire (2011), Coseismic and postseismic slip of the 2011 magnitude-9 Tohoku-Oki earthquake, *Nature*, *475*, 373–376, doi:10.1038/nature10227.

Pollitz, F. F., R. Bürgmann, and P. Banerjee (2011), Geodetic slip model of the 2011 M9.0 Tohoku earthquake, *Geophys. Res. Lett.*, *38*, L00G08, doi:10.1029/2011GL048632.

Satake, K. (1995), Linear and nonlinear computations of the 1992 Nicaragua earthquake tsunami, *Pure Appl. Geophys.*, *144*, 455–470, doi:10.1007/BF00874378.

Sato, M., T. Ishikawa, N. Ujihara, S. Yoshida, M. Fujita, M. Mochizuki, and A. Asada (2011), Displacement above the hypocenter of the 2011 Tohoku-Oki earthquake, *Science*, *332*(6036), 1395, doi:10.1126/science.1207401.

Sawai, Y., Y. Fujii, O. Fujiwara, T. Kamataki, J. Komatsubara, Y. Okamura, K. Satake, and M. Shishikura (2008), Marine incursions of the past 1500 years and evidence of tsunamis at Suijin-numa, a coastal lake facing the Japan Trench, *Holocene*, *18*(4), 517–528, doi:10.1177/0959683608089206.

Seno, T., K. Shimazaki, P. Somerville, K. Sudo, and T. Eguchi (1980), Rupture process of the Miyagi-oki, Japan, earthquake of June 12, 1978, *Phys. Earth Planet. Inter.*, *23*, 39–61.

Shao, G., X. Li, C. Ji, and T. Maeda (2011), Focal mechanism and slip history of 2011 M_w 9.1 off the Pacific coast of Tohoku earthquake, constrained with teleseismic body and surface waves, *Earth Planets Space*, *63*(7), 559–564, doi:10.5047/eps.2011.06.028.

Shibazaki, B., T. Matsuzawa, A. Tsutsumi, K. Ujiie, A. Hasegawa, and Y. Ito (2011), 3D modeling of the cycle of a great Tohoku-Oki earthquake, considering frictional behavior at low to high slip velocities, *Geophys. Res. Lett.*, *38*, L21305, doi:10.1029/2011GL049308.

Simons, M., et al. (2011), The 2011 magnitude 9.0 Tohoku-Oki earthquake: Mosaicking the megathrust from seconds to centuries, *Science*, *332*(6036), 1421–1425, doi:10.1126/science.1206731.

Tamura, Y., T. Sato, M. Ooe, and M. Ishiguro (1991), A procedure for tidal analysis with bayesian information criterion, *Geophys. J. Int.*, *104*(3), 507–516.

Uchida, N., and T. Matsuzawa (2011), Coupling coefficient, hierarchical structure, and earthquake cycle for the source area of the 2011 Tohoku earthquake inferred from small repeating earthquake data, *Earth Planets Space*, *63*, 675–679, doi:10.5047/eps.2011.07.006.

Uchida, N., J. Nakajima, A. Hasegawa, and T. Matsuzawa (2009), What controls interplate coupling?: Evidence for abrupt change in coupling across a border between two overlying plates in the ne japan subduction zone, *Earth Planet. Sci. Lett.*, *283*, 111–121, doi:10.1016/j.epsl.2009.04.003.

Umino, N., T. Kono, T. Okada, J. Nakajima, T. Matsuzawa, N. Uchida, A. Hasegawa, Y. Tamura, and G. Aoki (2006), Revisiting the three M $\sim$ 7 Miyagi-Oki earthquakes in the 1930s: Possible seismogenic slip on asperities that were re-ruptured during the 1978 M = 7.4 Miyagi-Oki earthquake, *Earth Planets Space*, *58*(12), 1587–1592.

Wessel, P., and W. Smith (1998), New, improved version of Generic Mapping Tools released, *Eos Trans. AGU*, *79*, 579.

Yabuki, T., and M. Matsu'ura (1992), Geodetic data inversion using a Bayesian information criterion for spatial distribution of fault slip, *Geophys. J. Int.*, *109*, 363–375.

Yagi, Y., and Y. Fukahata (2011), Rupture process of the 2011 Tohoku-Oki earthquake and absolute elastic strain release, *Geophys. Res. Lett.*, *38*, L19307, doi:10.1029/2011GL048701.

Yamamoto, Y., R. Hino, and M. Shinohara (2011), Mantle wedge structure in the miyagi prefecture forearc region, central northeastern Japan arc, and its relation to corner-flow pattern and interplate coupling, *J. Geophys. Res.*, *116*, B10310, doi:10.1029/2011JB008470.

Yamanaka, Y., and M. Kikuchi (2003), Source process of the recurrent Tokachi-Oki earthquake on September 26, 2003, inferred from teleseismic body waves, *Earth Planets Space*, *55*, e21–e24.

Yamanaka, Y., and M. Kikuchi (2004), Asperity map along the subduction zone in northeastern Japan inferred from regional seismic data, *J. Geophys. Res.*, *109*, B07307, doi:10.1029/2003JB002683.